Pelagic–benthic coupling within an upwelling system of the subtropical northeast Atlantic over the last 35 ka BP

C.L. McKay [a,*], H.L. Filipsson [a], O.E. Romero [b], J.-B.W. Stuut [c,b], B. Donner [b]

[a] Department of Geology, Lund University, Sölvegatan 12, SE-223 62 Lund, Sweden
[b] MARUM – Center for Marine Environmental Sciences, Universität Bremen, Leobener Strasse, 28359 Bremen, Germany
[c] NIOZ – Royal Netherlands Institute for Sea Research, Marine Geology Department, P.O. Box 59, NL-1790 AB Den Burg, The Netherlands

ABSTRACT

We present a high resolution, multiproxy study of the relationship between pelagic and benthic environments of a coastal upwelling system in the subtropical NE Atlantic Ocean. Marine sediments corresponding to late MIS3 to the Holocene in the radiocarbon dated core GeoB7926, retrieved off Mauritania (21°N) were analysed to reconstruct productivity in surface waters and its linkage to deep waters during the last 35 ka BP. High latitude cold events and changes in atmospheric and oceanographic dynamics influenced upwelling intensity over this time period. Subsequently, this caused changes in primary productivity off this low-latitude coastal upwelling locality. The benthic foraminiferal fauna displays four main community shifts corresponding to fundamental climatic events, first of all during late MIS3 (35 −28 ka BP), secondly from 28 to 19 ka BP (including Heinrich event 2 and the LGM), thirdly within Heinrich event 1, the Bølling Allerød and the Younger Dryas (18−11.5 ka BP) and finally during the Holocene (11.5–0 ka BP). In particular, strong pelagic–benthic coupling is apparent in MIS 3, as demonstrated by increased primary productivity, indicated by moderate DAR and the dominance of benthic foraminiferal species which prefer fresh phytodetritus. A decline in upwelling intensity and nutrient availability follows, which resulted in a proportionately larger amount of older, degraded matter, provoking a shift in the benthic foraminifera fauna composition. This rapid response of the benthic environment continues with a progressive increase in upwelling intensity due to sea level and ocean-ographic changes and according high surface production during the LGM. During Heinrich event 1 and the Younger Dryas, extreme levels of primary production actually hindered benthic environment through the development of low oxygen conditions. After this period, a final change in benthic foraminiferal community composition occurs which indicates a return to more oxygenated conditions during the Holocene.

© 2014 Elsevier Ltd. All rights reserved.

1. Introduction

Coastal upwelling zones exhibit high productivity which plays an integral role in biogeochemical cycles and marine ecosystems. One of the highest productive upwelling systems of the world ocean is located off the coast of Mauritania, in the subtropical NE Atlantic. The rationale for this study is to increase our understanding of how the marine environment within this subtropical upwelling setting responded to past rapid climate change, in this case, during the last 35 ka BP. Here, for the first time, direct accounts of how the benthic environment reacted to export productivity and climatic variations are addressed as well as the roles

of other parameters such as upwelling source. Furthermore, little is known about the relationship between surface and benthic productivity in this context. This is due to a lack of suitable high resolution cores and the availability of appropriate proxy data.

Several late Quaternary records from the NE subtropical Atlantic have shown that environmental conditions and upwelling intensity varied during the last deglaciation and the Holocene (McGregor et al., 2007; Romero et al., 2008). Such reconstructions have illustrated abrupt, large-scale changes along this upwelling system (eg. Kim et al., 2007). For example, during the Last Glacial Maximum (LGM) sea surface temperatures were warmer, upwelling was weaker and marine productivity was lower, when compared to the previous older glacial and subsequent deglaciation periods (Zhao et al., 2000). In general, primary productivity variations in coastal upwelling areas have regularly been accredited to changes in wind stress. However, the productivity dynamics at the site of GeoB7926

* Corresponding author. Tel.: +46 462227881.
  E-mail address: Claire.McKay@geol.lu.se (C.L. McKay).

are more multifaceted because of the complex atmospheric and hydrographic setting (Mittelstaedt et al., 1975). Located at an important climatic transition region of the Intertropical Convergence Zone (ITCZ), changes in surface productivity and subsequent export production are interlinked with past climate and oceanographic changes at this locality and we propose that subsequently, this strongly impacts the underlying benthos. Climate transitions and surface productivity off the coast of NW Africa have previously been studied extensively (e.g. Abrantes, 2000; Zhao et al., 2000; Romero et al., 2008), however the response of the benthic environment has received little attention.

Benthic foraminifera serve as an important tool for reconstructing past deep sea environments. In most open-ocean settings, food availability associated with sea surface primary production and oxygen availability are key limiting factors which determine benthic communities (Gooday, 1988; Schnitker, 1994; Gooday and Jorissen, 2012). Hence by studying faunal densities, species compositions and diversity parameters it is possible to reconstruct the surface productivity changes as well as the former benthic conditions whilst taking into account taphonomic processes as well as changes in export capacity (Jorissen, 1999). Moreover, organic input is interconnected with oxygen levels as a high organic accumulation can lead to oxygen depletion of the bottom- and sediment pore water which in turn can play a role in determining the vertical distribution of benthic foraminifera and the taxa present (Jorissen, 1999). In particular, the benthic environment of site GeoB7926 was studied in terms of oxygenation conditions at the sea floor since the last deglaciation (Filipsson et al., 2011). The benthic foraminiferal faunal assemblage data is extended here in order to further assess benthic regime shifts further back in time, during the late Marine Isotope Stage 3 (MIS3), Heinrich event 2 (H2), the Last Glacial Maximum (LGM), Heinrich event 1 (H1) in more detail and the Holocene. Furthermore we compare the results with other productivity studies from upwelling sites within the subtropical NE Atlantic.

Here we extend the work of Romero et al. (2008) and Filipsson et al. (2011) to provide a better understanding of pelagic–benthic coupling and present a detailed multiproxy reconstruction. This multiproxy approach enables the study of prospective affiliation between palaeoproductivity and palaeoenvironmental indicators (benthic foraminifera, diatoms, opal, total organic carbon and CaCO₃) with wind strength, upwelling intensity and climate of the adjacent land mass (Ti/Ca ratios, grain-size analysis and end-member modelling) from marine sediment core GeoB7926 from the continental slope off the coast of Mauritania Furthermore, this study is of global relevance since upwelling intensity and primary productivity have varied considerably during the last deglaciation (Romero et al., 2008; Gallego-Torres et al., 2014). Therefore it is of great interest to investigate how the benthic environment responded to high latitude climate events, larger scale circulation changes in the NE Atlantic and according changes in export production.

2. Regional settings

2.1. Climate

The atmospheric circulation patterns and climate in this coastal region are driven by the NE trade winds and the easterly Saharan Air Layer (SAL) (Prospero and Carlson, 1981) with interplay of the Azores high pressure cell (Moreno, 2012). The trade wind strength and trajectories and according upwelling intensity are primarily dependent on seasonal ITCZ displacement (Mittelstaedt, 1991). During boreal summer, the ITCZ has a northerly position, whereas during winter it has a more southerly position (Nicholson, 1986). This in turn influences the temporal dynamics of productivity by

controlling nutrient availability sourced from the influx of terrestrial dust and upwelled nutrients.

2.2. Oceanography

As part of the NE Atlantic Boundary Current System (EBCS), a principal feature off the coast of the NW African continent is coastal upwelling of cool, nutrient-rich subsurface water. This region is one of the key upwelling areas in the world ocean. Offshore of Mauritania, almost year-round upwelling occurs at the shelf (Schemainda et al., 1975). The combined effect of the Coriolis effect and the NE trade winds promotes Ekman transport which also forms offshore extending upwelling filaments. This further enhances surface water productivity of the coastal area (Helmke et al., 2005).

This upwelling system is characterised by significant seasonal and regional features which results in differences in the surface water primary productivity and export production to the benthos (Jorissen and Wittling, 1999). Two areas of high primary production occur (Jorissen et al., 1998); one high productivity patch is located at the outer shelf which corresponds to the year-round upwelling (Schemainda et al., 1975) and the second is situated several hundred kilometres offshore. The latter productivity maximum is caused by a hydrographic gradient during summer whereby the offshore east-west deviation of the CC is strengthened, which also contributes to the transportation of nutrients offshore (Mittelstaedt, 1983).

The main surface current; the southward-flowing Canary Current (CC) is linked to the atmospheric circulation along the northwest continental African margin (Mittelstaedt, 1991; Pelegrí et al., 2005). The CC is underlain by subsurface waters masses which ascend into the surface layers through the upwelling process (Mittelstaedt, 1991). A transition exists just north of Cape Blanc (24°N) whereby to the north, North Atlantic Central Water (NACW) is an important constituent of the upwelled waters and to the south of this convergence, the upwelled waters contain a significant portion of South Atlantic Central Waters (SACW). Southward-flowing, deeper-running NACW (Fütterer, 1983) is nutrient depleted in comparison to the northward-flowing SACW, which is less saline and more nutrient rich (Gardener, 1977). At intermediate layers, water masses are composed of the Antarctic Intermediate Waters (AAIW; between 600 and 1000 m), Mediterranean and Arctic Intermediate waters down to 1500 m (Knoll et al., 2002). Below 1500 m, North Atlantic deep water (NADW) is present (Lutze and Coulbourn, 1983) and below 4000 m, northward flowing Antarctic Bottom water (AABW) is present (Sarnthein et al., 1982).

In addition, the site studied (Fig. 1) is located at the convergence of the different upwelling waters; the nutrient enriched SACW and the nutrient depleted NACW. The periphery of this convergence migrates in position (Mittelstaedt, 1991) and hence the source of the upwelled water changes with wind trajectories. Also, the extension and dimension of the upwelling filaments depend on the coastal and seafloor morphology as well as the wind induced upwelling intensity (Hagen et al., 1996). Off the shelf edge, the sea floor morphology is characterised by numerous trenches and large canyons (Fütterer, 1983; Krastel et al., 2004).

3. Material and methods

3.1. Gravity core GeoB7926-2

Our study focusses on gravity core GeoB7926-2, retrieved off northwest Africa on the continental slope 200 km off the Mauritanian coastline (Fig. 1), during Meteor cruise M53/1 (20°13′N,
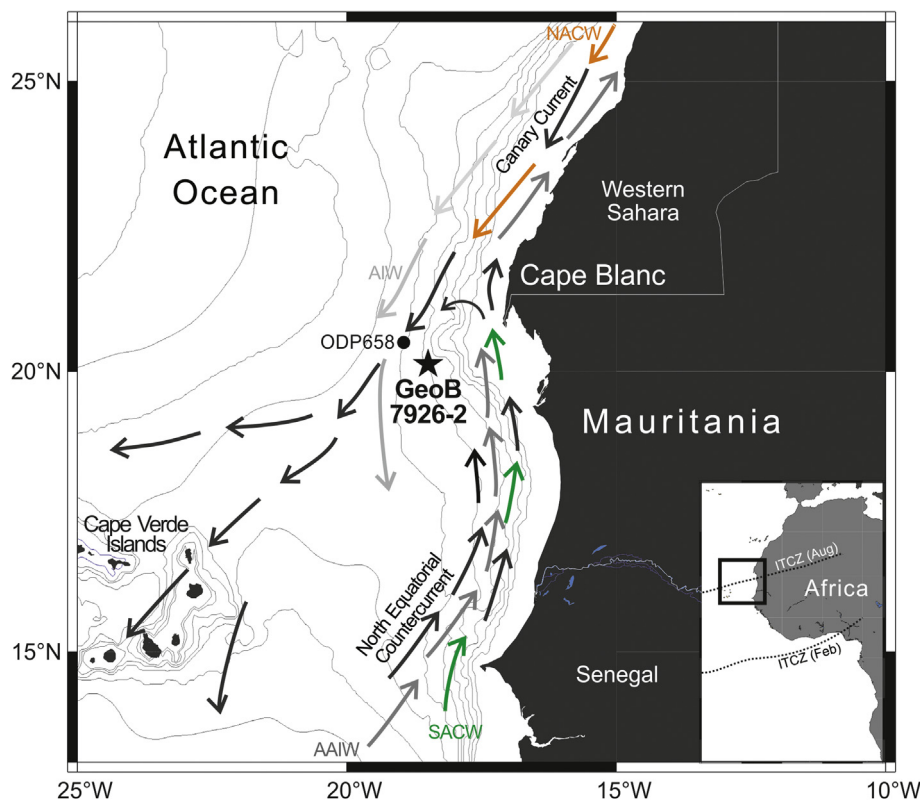
Fig. 1. Location of core GeoB7926-2 (black star) off the coast of Mauritania in the NE Atlantic Ocean. The proximity of site ODP658 (black dot) is also shown. Arrows indicate the currents and water masses. Black arrows show surface water circulation (Canary Current and North Equatorial Countercurrent), orange show North Atlantic Central Water (NACW), green show South Atlantic Central Water (SACW), light grey show Arctic Intermediate Water (AIW) and dark grey show Antarctic Intermediate Waters (AAIW). Inset is the present day position of the ITCZ for August and February (Romero et al., 2008).

18°27′E, 2500 m water depth); (Meggers and Cruise Participants, 2003). The 1328 cm long sediment core mainly consists of a foraminifera bearing nannoplankton or diatomaceous ooze. A detailed core description was published by Meggers and Cruise Participants (2003) and Romero et al. (2008).

Sediment samples were prepared for microfaunal analysis, stored and are archived at MARUM (University of Bremen, Germany). In this work, we present new results corresponding to the period 18–35 ka (608 cm–1078 cm), we also include data from Filipsson et al. (2011); whereby 0–18 ka (upper 600 cm) was investigated with respect to benthic foraminifera and Romero et al. (2008) focussing on the pelagic production of 0–25 ka (the upper 820 cm).

3.2. Chronology

The age model for the core GeoB7926-2 is based on 16 accelerator mass spectrometric (AMS) ^{14}C age determinations (Table 1, Fig. 2) analysed on the planktonic foraminifera *Globigerina inflata* (>150 μm fraction) (Kim et al., 2012). In order to increase the temporal resolution and confirm robustness of the age model originally constructed by Romero et al. (2008) and revised by Kim et al. (2012), four additional AMS ^{14}C ages were determined at the Radiocarbon Laboratory at Lund University, Sweden (Table 1). The new radiocarbon dates were converted into calendar years using the CALIB REV6.0.0 program with the marine calibration dataset MARINE09 (Reimer et al., 2009). As regional reservoir ages are unknown for this upwelling setting, a mean ocean reservoir age of 400 years (Bard, 1988) was employed however, we acknowledge that regional reservoir ages may be larger and may have changed overtime due to the upwelling of older subsurface waters and changes in upwelling intensity

(deMenocal et al., 2000a). The termination of MIS3 is defined at 28 ka and the LGM is marked between 23 and 19 ka. The Bølling Allerød (BA) and Younger Dryas (YD) are temporally defined at 15.5–13.5 ka BP and 13.5–11.5 ka BP respectively, after Romero et al. (2008), Filipsson et al. (2011) and Kim et al. (2012). The conventionally accepted scheme of event terminology employed here reflects their marine and terrestrial expression. For this INTIMATE special issue, we acknowledge that the climatic terms are applied as follows after Rasmussen et al. (submitted): LGM: GS2.1, B-A: GI-1 and YD: GS-1.

3.3. Diatom analysis

Diatom data has previously been presented by Romero et al. (2008) for the interval 0–25 ka BP. Within this work we extend the diatom record back in time to 35 ka BP, with sampling continuing at 5 cm intervals, following preparation and counting methods of Schrader and Gersonde (1978). Further details of the qualitative and quantitative analyses are published in Romero et al. (2008). Total diatom concentration includes all marine diatoms plus freshwater species. The relative contribution of non-marine diatoms and benthic species remain low; below 1% and 3% respectively. The most abundant diatom species were assigned to three groups representing 1: strong coastal upwelling, 2: moderate coastal upwelling and 3: low productive conditions by following well-known ecological information from low- and mid-latitude ocean settings. To account for the changing sedimentation rate, diatom accumulation rates (DAR) were calculated as follows: DAR (number of valves $cm^{-2}\,ka^{-1}$) = $D \times SAR$ where D is the number of diatom valves per cm^3 of sediment, SAR is the sediment accumulation rate (cm/ka).

Table 1
21 Acceleration mass spectrometer ^{14}C dates and calibrated calendar dates (ka BP) of gravity core GeoB7926-2.

| Lab no.	Depth in core (cm)	Uncorrected AMS ^{14}C ages (yr BP)	Analytical error (±1σ) (yrs)	Age ((ΔR = 0 yr) (±2σ)) (yr BP)	Calibrated: Oxcal (ka BP)	Age (ka BP) age model: Kim et al. (2012)	Analysed material	Reference
KIA 24287	8	1170	35	649–787	0.708	0.718	G. inflata	Romero et al. (2008)
KIA 25812	48	4455	35	4519–4779	4.578	4.649	G. inflata	Romero et al. (2008)
KIA 25810	98	8970	45	9515–9798	9.521	96.565	G. inflata	Romero et al. (2008)
KIA 24286	173	10,830	70	12,054–12,560	11.426	12.307	G. inflata	Romero et al. (2008)
KIA 22417	248	11,020	60	12,357–12,677	12.427	12.517	G. inflata	Romero et al. (2008)
KIA 24285	378	12,220	70	13,450–13,824	14.003	13.637	G. inflata	Romero et al. (2008)
KIA 29030	418	13,050	70	14,487–15,247	14.921	14.867	G. inflata	Romero et al. (2008)
KIA 27310	483	13,720	100	15,568–16,813	16.439	16.190	G. inflata	Romero et al. (2008)
KIA 29029	508	14,290	60	16,777–17,166	16.876	16.972	G. inflata	Romero et al. (2008)
KIA 22416	553	14,670	80	16,990–17,686	17.265	17.338	G. inflata	Romero et al. (2008)
LuS 9530	608	14,900	120	18,322–18,524	18.425	18.112	G. inflata	This study
KIA 27309	688	16,600	130	18,903–19,571	20.096	19.237	G. inflata	Romero et al. (2008)
LuS 9531	723	18,150	130	21,000–21,502	21.263	20.667	G. inflata	This study
KIA 29028	803	20,450	160	23,484–24,388	24.202	23.936	G. inflata	Romero et al. (2008)
KIA 24283	868	23,650	230	27,562–28,622	27.252	28.092	G. inflata	Romero et al. (2008)
LuS 9532	963	27,425	350	30,945–31,428	31.179	31.024	G. inflata	This study
KIA 22415	1053	29,600	360	32,949–34,654	33.979	33.802	G. inflata	Kim et al. (2012)
LuS 9533	1123	29,850	350	36,000–36,389	36.177	36.899	G. inflata	This study
KIA 27308	1203	36,440	1400	37,740–43,136	40.414	40.438	G. inflata	Kim et al. (2012)
LuS 9534	1208	39,429	2500	39,647–41,190	40.414	40.761	G. inflata	This study
KIA 24282	1323	45,410	360	46,857–49,503	40.669	48.180	G. inflata	Kim et al. (2012)
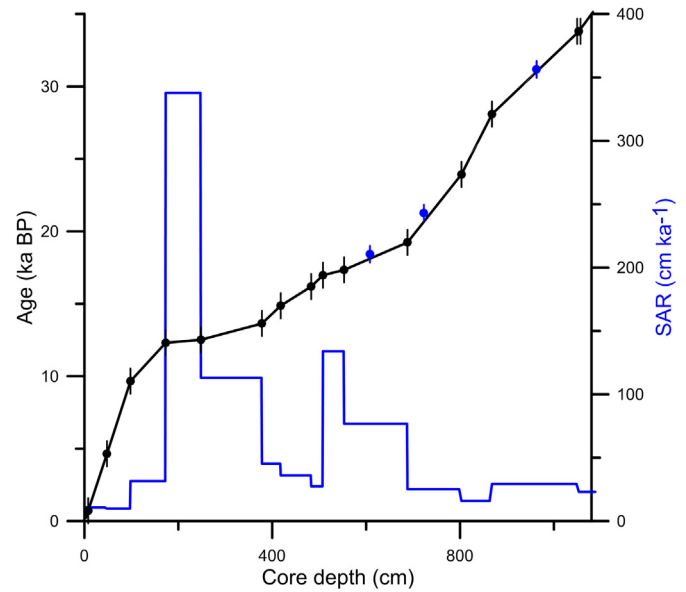
Fig. 2. Age model (black line) obtained from 16 calibrated ^{14}C dates and sediment accumulation rates (cm ka^{-1}) from 35 ka to present for upper 1080 cm of core GeoB7926-2 (Romero et al. 2008; Kim et al. 2012). Blue circles denote new ^{14}C dates. Absolute values are summarised in Table 1. (For interpretation of the references to colour in this figure legend, the reader is referred to the web version of this article.)

3.4. Benthic foraminifera assemblage analysis

For benthic foraminiferal faunal analyses, 10 cm^3 of sediment was sampled, freeze-dried, wet sieved over >63 μm and >150 μm sieves and oven dried at 40 °C. Using the >150 μm fraction, faunal analyses of 300 specimens were determined to the species level. This was undertaken at 10 cm resolution and higher (5 cm) where high surface productivity was apparent, on samples corresponding to 18–35 ka BP to extend the previous dataset of Filipsson et al. (2011). Counts were adjusted accordingly for split samples and taxonomic identification follows Loeblich and Tappan (1987) and Jones (1994). We acknowledge that smaller foraminifera may be important (Schröder et al., 1987) and therefore, the 63–150 μm fraction was observed to check for consistent faunal similarities. Overall, the same species were noted in the 63–150 μm fraction as in the 150 μm but smaller species were naturally in higher abundance. The general faunal characteristics are expressed as Shannon diversity and dominance (percentage of most frequent species). Taxa that displayed abundances of ≥5% were selected for statistical analyses. To account for the changing sedimentation rate, benthic foraminifera accumulation rates (BFAR) were calculated as follows: BFAR (number of specimens cm^{-2} ka^{-1}) = BF × SAR where BF is the number of benthic foraminifera specimens per cm^3 of sediment, SAR is the sediment accumulation rate (cm/ka).

In order to distinguish the composition of benthic foraminiferal assemblages and to highlight changing species dominance through the GeoB7926-2 record, we applied a CABFAC factor analysis with Varimax rotation using the software PAST (Hammer et al., 2001). The analysis included all species with relative abundances ≥5% in at least one sample. To detect which environmental variables were influencing the foraminiferal assemblages, BEST (Bio-Env + Stepwise) tests were performed for each time interval individually using the software PRIMER (Clarke and Gorley, 2006). BEST analysis was the selected procedure because it calculates the correlation between the multivariate among-sample patterns of abundance data and that from environmental variables associated with those samples. All species ≥5% were included and normalised

and the environmental variables included were diatom concentration, opal and TOC content, mean grain-size and the following elemental counts: Ti, K, Mn, Fe, Cu and Sr. BEST analysis results were tested for significance at $\rho < 1\%$.

3.5. Bulk geochemistry

Bulk geochemical analyses for the last 25 ka BP were published in Romero et al. (2008) and here we extend the record back to 35 ka BP as proxies of productivity. Samples were taken at 5 cm intervals, freeze dried and ground in an agate mortar. After decalcification of the samples with 6 N HCl, the total organic carbon (TOC) content was determined by combustion at 1050 °C. Carbonate ($CaCO_3$) was calculated from the difference between total carbon and TOC and expressed as calcite. Opal content was obtained using the sequential leaching technique of DeMaster (1981) with adjustments by Müller and Schneider (1993).

3.6. X-Ray Fluorescence (XRF) scanning

XRF scanning is a non-destructive method for high-resolution analyses of elemental intensities in counts per second (cps). Scanning was undertaken at MARUM (Bremen) on the split cores at 1 cm intervals in the upper 350 cm of GeoB7926-2 and every 2 cm thereafter; from 350 cm downcore. From the whole set of elements measured, we show here Ti/Ca as a proxy for wind strength and according upwelling intensity. Calcium (Ca) mainly reflects the biogenic carbonate content whereas titanium (Ti) is related to siliciclastic sediment components and varies directly with the terrigenous fraction of the sediment (Arz et al., 1998; Tjallingii et al., 2008). As well as Ti, we also utilise the following elemental counts for testing for correlations with benthic foraminiferal abundance data: K and Sr as proxies of aeolian dust input and the redox sensitive elements Mn, Fe, and Cu to infer potential foraminifera abundance patterns with past oxygen levels. XRF data for the last 25 ka BP has previously been published (Romero et al., 2008) and here we extend the record back to 35 ka BP. We log transform the elemental ratios as recommended by Weltje and Tjallingii (2008). Using a simple linear transformation enables a more easily interpretable signal of relative changes in chemical composition and minimises the risk of drawing inaccurate conclusions.

3.7. Grain-size analysis and end-member modelling

To determine the origin of the terrigenous fraction, grain-size analysis and subsequently end-member modelling were utilised. Here, we use mean particle size as a proxy of wind strength and the end-members as proxies of terrestrial humidity (fine, fluvial muds) and wind strength (coarser fraction). 0.5 g of sediment was subsampled at 5 cm intervals and the biogenic compounds were removed from the sediment. Organic carbon was removed by heating the sample to 100 °C in H_2O_2 (35%). Subsequently, the samples were treated for 1 min with HCl (10%) at 100 °C to remove $CaCO_3$ and biogenic opal was removed with NaOH. Measurements were performed in demineralised and degassed water in order to improve the signal-to-noise ratio of the particle-size analysis. Grain-size distributions were measured using a Beckman Coulter laser particle sizer LS200, resulting in 92 size classes ranging from 0.4 to 2000 μm. All pretreatments and the grain-size measurements were completed at MARUM (Bremen) and data for 0 to 18 ka BP was previously published in Filipsson et al. (2011). Here we extend this data back to 35 ka BP. Numerical end-member modelling was employed to differentiate distinctive sediment subpopulations within the grain-size distribution. Samples

corresponding to turbidites (Meggers et al., 2003) were not included in order to avoid misrepresentation of the coarse fraction from sediment originating from the continental shelf. The algorithm EMMA was used (Weltje, 1997) and the end-members chosen based on the goodness of fit statistics by calculating the coefficient of determination (r^2) which represents the quantity of variance of each grain-size class that can be replicated by the approximated data, as documented in Filipsson et al. (2011). The outcome of the model represents real particle-size distributions whose end-members are a statistically unique solution. Further details are provided in Weltje and Prins (2003).

4. Results

4.1. Age model

The new radiocarbon ages fit well within the error margins of the age model (Fig. 2, Table 1). Therefore after substantial revisions of the age model in conjunction with these new ages, we can reaffirm the reliability of the age model. GeoB7926 is characterised by an unusually high sedimentation rate of $\sim$96 cm ka^{-1} with highest sedimentation rates ranging between $\sim$110 and $\sim$320 cm ka^{-1} during H1 and YD (Fig. 2).

4.2. Diatom assemblages

The diatom assemblage is highly diverse at site GeoB7926. At least 200 diatom species were identified and throughout the core the assemblages are dominated by resting spores of *Chaetoceros*. Relatively high diatom accumulation occurs during late MIS3 peaking at 33.8 ka BP with 6.3×10^7 valves cm^{-2}. Later DAR progressively increases over the course of the LGM with highest accumulation values during late H1 and the YD, exceeding values of 6.8×10^7 and 6.4×10^7 valves cm^{-2} at 16.5 and 12.9 ka BP respectively. As previously shown by Romero et al. (2008), sedimentation rate correlates well with diatom concentrations and so, the high DARs seen in this record are not merely an effect of the high sedimentation rates.

Fig. 3 shows the temporal distribution of three main diatom groups: species associated with (1) strong coastal upwelling, (2) moderate coastal upwelling, and (3) pelagic, warm waters, low productive conditions. Resting spores (RS) of *Chaetoceros affinis* and *Chaetoceros diadema* contribute to group 1 and their downcore distribution mostly matches well with temporal variations of total diatom concentration (Fig. 3). Species of the moderate upwelling group (RS of *Chaetoceros compressus*, *Chaetoceros debilis*, *Chaetoceros seychellarum*, and spores of an unidentified *Chaetoceros*) are most abundant during periods of lessened diatom production and its contribution tends to be highest when group 1 contribution decreases. Diatoms of warm, pelagic, low-productive waters, mainly *Actinoptychus* spp., *Coscinodiscus radiatus*, *Fragilariopsis doliolus*, and *Planktoniella* sol; (Romero et al., 2008) contribute the most between 13.5 ka BP and the latest Holocene.

4.3. Benthic foraminiferal faunal assemblages

Site GeoB7926 documents both rapid and continuous changes in benthic productivity and the environmental conditions during the last 35 ka BP. More than 100 benthic foraminifera species were identified within the time interval of 35 ka BP. Species with a relative abundance of over 3% are focussed on here and the most prominent species as displayed in Fig. 4. Several benthic foraminiferal species persist throughout the entire record including *Nonionella iridea*, *Melonis barleeanum* and *Cassidulina laevigata* but in varying abundance.
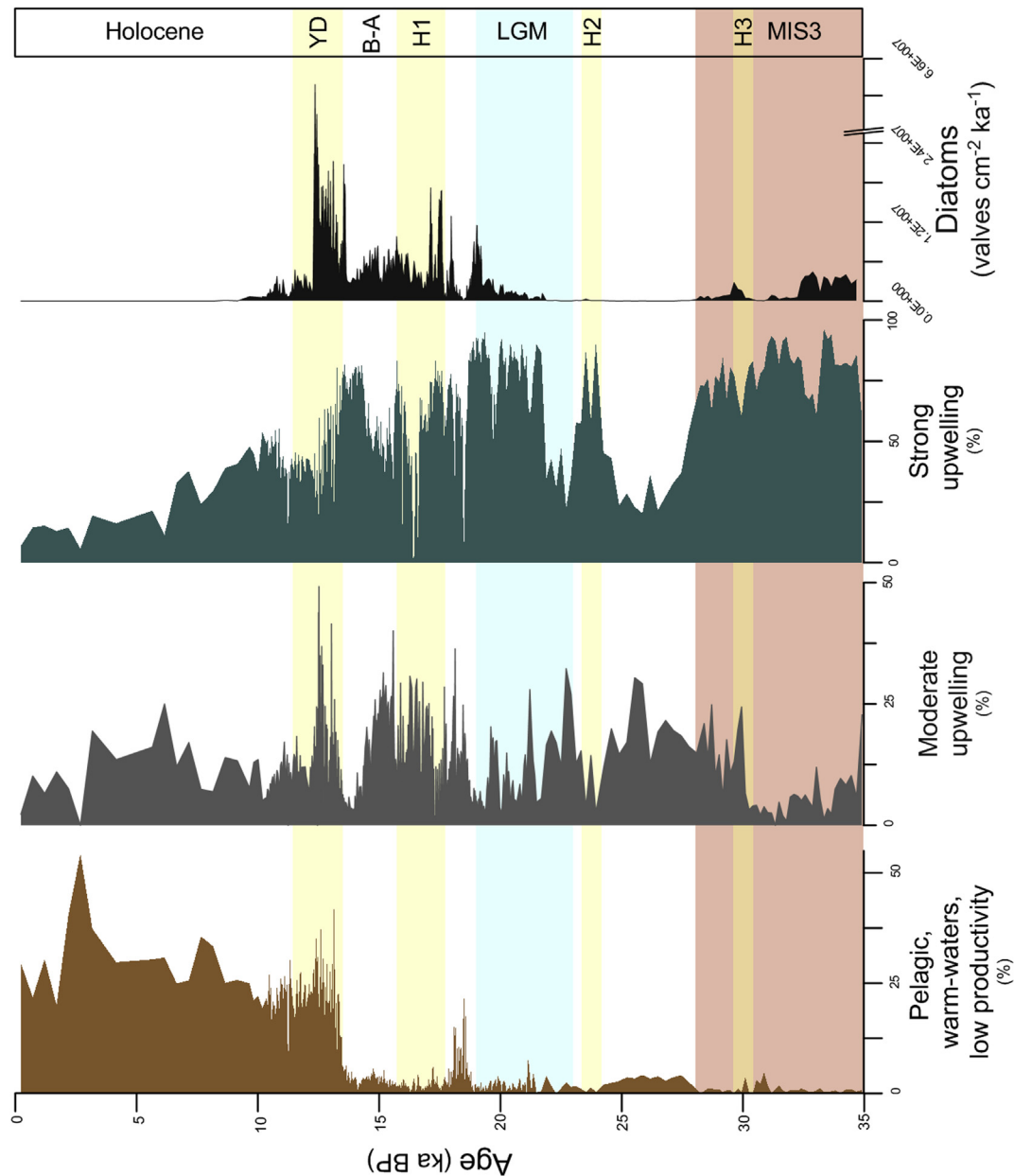
Fig. 3. The distribution of the three identified diatom groups associated with (1) strong coastal upwelling (2) moderate upwelling intensity and (3) low productivity conditions.

The benthic foraminiferal diversity of core GeoB7926 ranges from Shannon diversity H(S) values of 0.86–3.24 and exhibits short-term fluctuations throughout the core with the lowest diversity occurring during the YD (Fig. 4). The factor analysis resulted in 4 factors, explaining as much as 90% of variance consisting of nine important (score >−1 and >1) species (Table 2). The four factors can be partitioned into four foraminiferal assemblages, each named after the most significant species explaining each factor. Factor 1, (42%) of the variance, correspond to the species *N. iridea* and *Globocassidulina crassa* (synonymised taxa; *Cassidulina crassa*). Factor 2 accounted for 25% of the variance and is represented by only one species: *Eubuliminella exilis* (synonymised taxa: *Bulimina exilis*). Factor 3 (14% of variance) was attributed to an assemblage of *Chilostomella oolina*, *Cibicides wuellerstorfi*, *M. barleeanum*, *Melonis pompilioides* and *Uvigerina peregrina*. Finally, factor 4 (9% of variance) denoted *Cassidella bradyi* (synonymised taxa: *Fursenkoina bradyi* and *Virgulina bradyi*).

Overall as shown in Fig. 4, during the past 35 ka BP, this diverse benthic community displays shifts in abundance and productivity with four main assemblages, which was also confirmed by the factor analysis. The dominant species throughout late MIS3 (35–28 ka BP) is *C. bradyi* (average 45%), emphasised by factor 4. Species of less importance are *N. iridea* (20%) and *C. laevigata* (6%). During this time interval, abundance of *C. bradyi* reaches maximum values of 70% at 31.8 ka BP, and exhibits fluctuations around 45% on average throughout this time interval. During MIS3, the benthic foraminifera concentrations increase from comparatively low to more moderate levels and the BFAR reflect this (Fig. 4). Relatively gradual fluctuations in Shannon diversity H(S) are apparent, with values ranging from 1.25 to 2.3. As H3 does not temporally cover a sufficient number of benthic foraminiferal faunal data points, BEST analysis was not undertaken for this period but instead on MIS3 data points, particularly since from factor 4 we can consider *C. bradyi* to be the fundamental species of this period. Within MIS3,
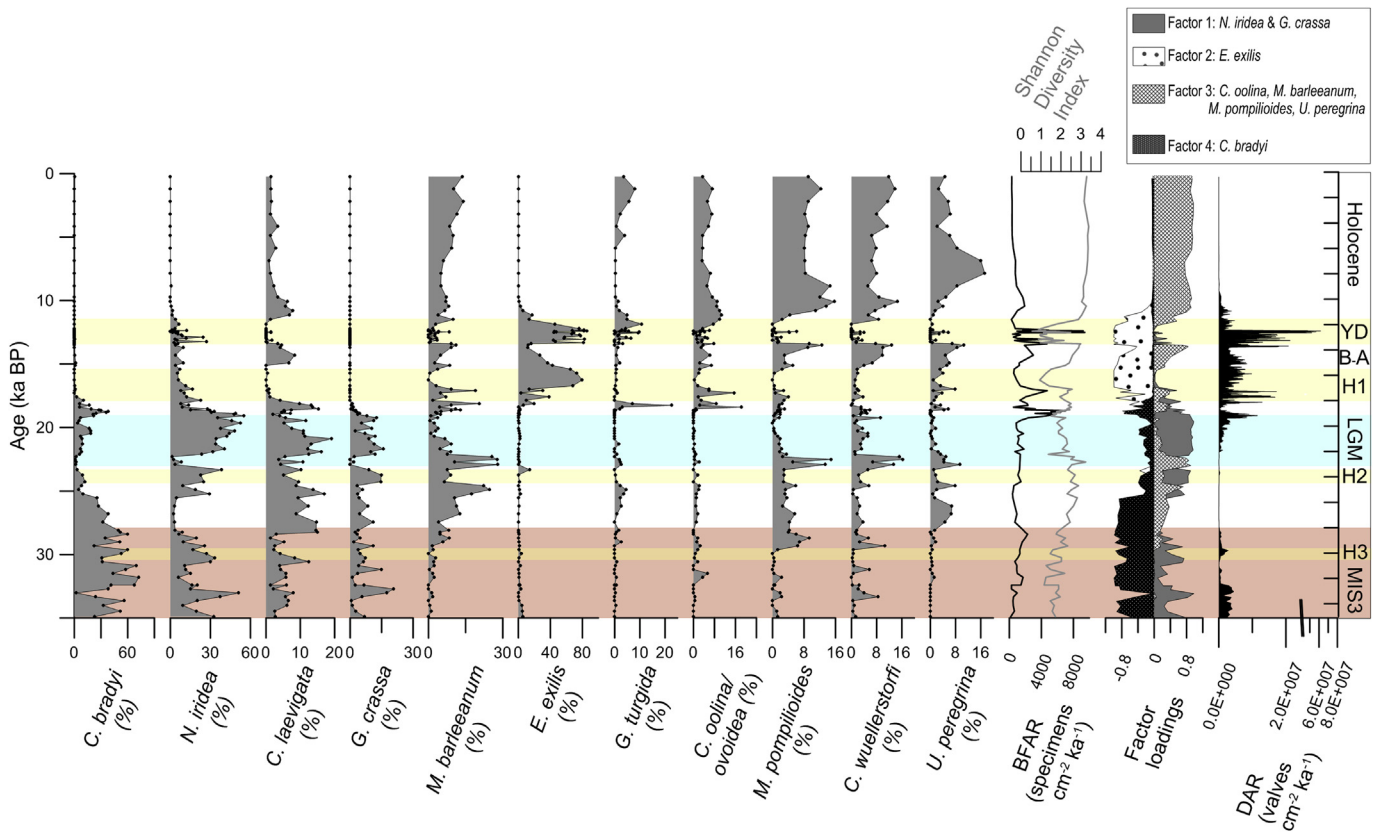
Fig. 4. GeoB7926-2 down-core changes in relative abundance (%) of the most common benthic foraminifera species (17−0 ka BP after Filipsson et al., 2011), benthic foraminiferal accumulation rate (specimens cm^{-2} ka^{-1}), Shannon diversity index, factor analysis loadings and diatom accumulation rate (valves cm^{-2} ka^{-1}). Shadings are as follows: light orange, late MIS3, (Marine Isotope Stage 3: 35-28 ka BP); light yellow, H3 (Heinrich event 3: 30.6-29.6 ka BP), H2 (Heinrich event 2: 24.5-23.25 ka BP), H1 (Heinrich event 1: 18−15.5 ka BP) and the YD (Younger Dryas; GS-1: 13.5−11.5 ka BP); light blue, LGM (Last Glacial Maximum; GS-2.1: 23−19 ka BP); unshaded B-A (Bølling-Allerød; GI-1: 15.5−13.5 ka BP) and the Holocene (11.5−0 ka BP). Note the different size x-axes of the benthic foraminiferal abundance data to emphasize the more abundant taxa. (For interpretation of the references to colour in this figure legend, the reader is referred to the web version of this article.)

the BEST analysis (Table 3) evaluates diatoms, TOC, K and Sr as the most important variables that explain the biotic patterns within the foraminifera abundance data.

At 28 ka BP, over H2 (24.25−23.25 ka BP) and the LGM (23−19 ka BP) *C. laevigata* and *M. barleeanum* become more abundant reaching 19 and 25% respectively. By H2, *C. bradyi* decreases in abundance whilst *N. iridea* remains dominant. The factor analysis highlights *N. iridea* and *G. crassa* (factor 1) to be most significant species within H2. The BFAR exhibits minor fluctuations and Shannon diversity H(S) values are comparatively higher at 2.8 prior to and during H2 in comparison to MIS3 and decrease to lower values of 2.16 on average over the course of the LGM. The BEST analysis of H2 suggests opal and K as the two abiotic variables matching the foraminifera abundance data whereas, for the LGM, the results suggest TOC, opal and Ti to be highly correlated (0.81).

A third community shift occurs during H1. During H1 and throughout the BA and the YD, an outstanding shift in species composition occurs, with several species, such as *C. bradyi* and *C. laevigata* being succeeded by *E. exilis*. At H1, *C. bradyi* is no longer present in the assemblage and *E. exilis* reaches 80% (at 16.5 ka BP) abundance in H1 and the YD which correlates with low Shannon diversity values as low as 0.9 and 0.56 respectively during these time intervals. From the BEST statistic results, we can see that the variables most associated with the benthic foraminifera faunal assemblage data changes over the course of this third assemblage (refer to Table 3), from opal playing a more dominant role in H1 and B-A to K and Mn in the YD.

A final assemblage change is seen during the Holocene where the benthos exhibits a high to low productivity pattern and diversity is high and virtually constant at H(S) values ca 3.3. *Melonis*

Table 2
Benthic foraminiferal assemblages revealed by factor analysis.

Factor	Variance (%)	Dominant species	Score
	Total variance 89.97		
1	42.07	*Globocassidulina crassa*	1.03
		Nonionella iridea	
2	24.8	*Eubuliminella exilis*	−4.95
3	14.33	*Melonis barleeanum*	2.64
		Melonis pompilioides	2.14
		Cibicides wuellerstorfi	2.07
		Uvigerina peregrina	2.28
4	8.77	*Cassidella bradyi*	−4.96

Table 3
BEST (Bio-Env + Stepwise) statistical analysis results: abiotic solutions explaining the variance of the relative foraminiferal abundance data for each individual climatic interval. All results are statistically significant at $\rho < 1\%$ except H2.

Interval	Variables	BEST ρ value
Late MIS3	Diatom concentration, TOC, K, Sr	0.39
H2	Opal, K	n.s
LGM	TOC, opal, Ti	0.81
H1	Opal, K, Ti, Sr	0.89
BA	TOC, opal, K, Fe	0.95
YD	K, Mn	0.57
Holocene	Mean grain-size, diatom concentration, opal, Fe	0.86

species dominate the assemblage and species which were previously low in abundance such as *Chilostomella sp.*, *C. wuellerstorfi*, *M. pompilioides* and *U. peregrina* increase during this recent time interval which is in accordance with factor 3 of the factor analysis. Within the Holocene, the BEST analysis (Table 3) evaluates mean grain-size, diatom concentration, opal and Fe as the most important variables that relate to the foraminifera abundance data.

4.4. TOC, CaCO₃ and biogenic opal content

Vast changes in sediment composition are recorded at site GeoB7926 (Fig. 5). The CaCO$_3$ content fluctuates between 30% and 55% since late MIS3 with an abrupt increase at the transition from the YD

into the Holocene. TOC content ranges between 0.38 and 3.55%, averaging at 1.84% over the entire studied interval. The late MIS3 is characterised by the highest TOC content, reaching 3.5% at 32.7 ka BP for example. TOC demonstrates a low- to high-productivity shift during H1 in this record and shows moderately low concentrations during the Holocene. Biogenic opal levels are moderate-low prior to H1, but reached high concentrations during H1 and the YD (up to 27% at 13 ka BP) with a subsequent decrease to low values in the Holocene.

4.5. Terrestrial component

We utilise ln Ti/Ca ratios as a proxy of wind strength which is highly variable on submillennial to millennial time scales at
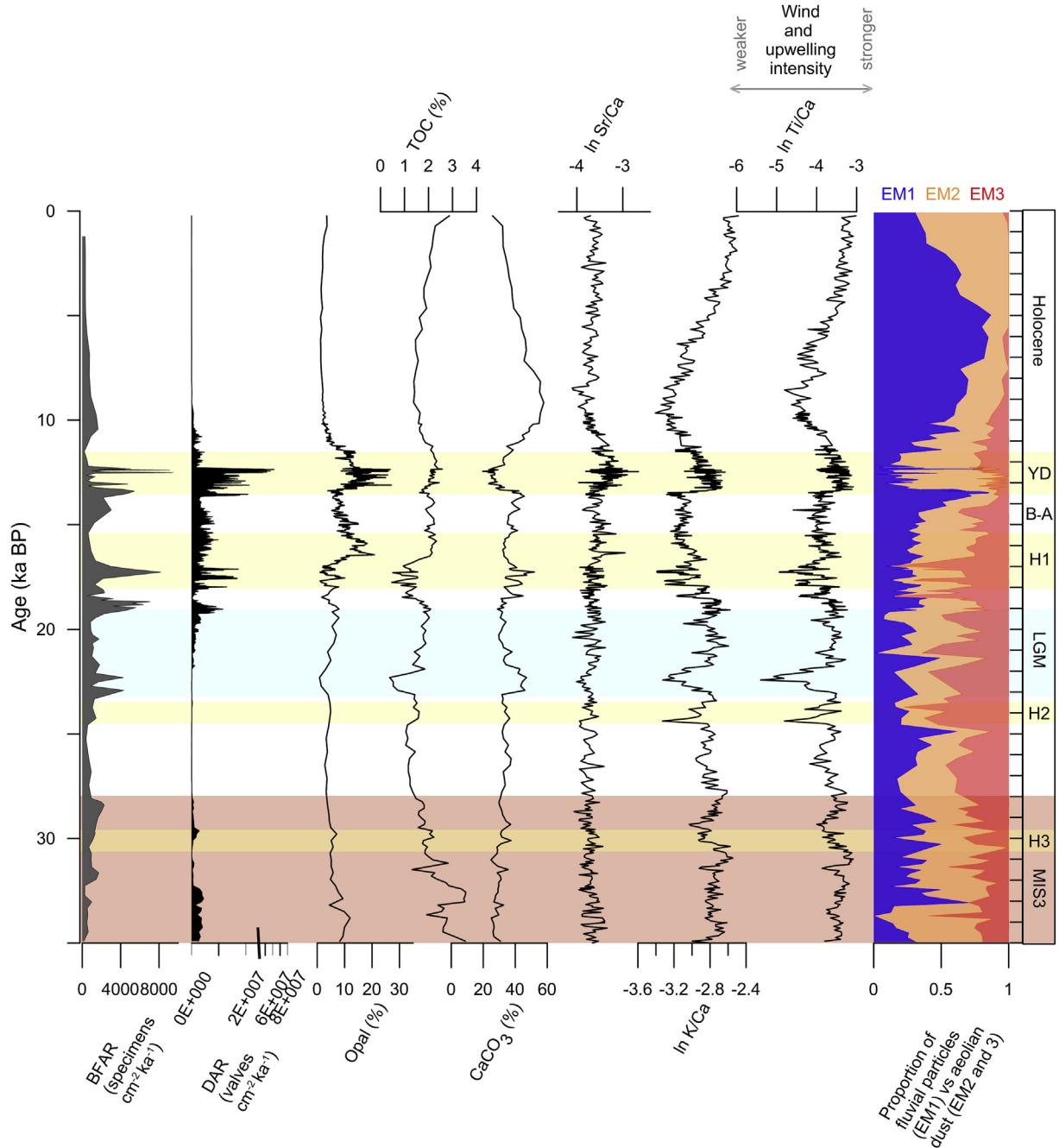

Fig. 5. GeoB7926-2 down-core variation of benthic foraminiferal accumulation rate (specimens cm^{-2} ka^{-1}), diatom accumulation rate (valves cm^{-2} ka^{-1}), TOC (%), CaCO$_3$ (%) biogenic opal (%), ln Sr/Ca, ln K/Ca, ln Ti/Ca values and proportions of end members (EM)1–3, where EM1 represents the fluvial component, EM2 and EM3 fine and coarse aeolian dust, respectively, presented with climatic time intervals (ka BP).

GeoB7926 (Fig. 5). Ti/Ca values ranged from 0.0045 to 0.046 with highest values during late MIS3 and the YD. As previously reported by Romero et al. (2008) Ti/Ca oscillates between 0.02 and 0.04 throughout the LGM and decreases in the early Holocene.

Grain-size analysis and end member modelling of the terrigenous fraction are utilised here to derive the provenance and confirm different sediment transport mechanisms. Within this region, grain-sizes of fluvial material are finer in comparison to aeolian dust (Koopmann, 1981) and hence we use mean particle size as a proxy of wind strength in tandem with end-members to infer the corresponding proportions of wind-blown sediment and riverine input from the coarsening and fining of grain-size respectively. Because of the locality of this site (Fig. 1), the terrigenous influx is supplied predominantly from the Sahara by the prevailing wind systems (Wilson, 1971; Sarnthein et al., 1982) and therefore the aeolian end members represent the carrying capacity and hence strength, of the winds.

Moderate particle range is revealed in the late MIS3 with relatively high grain-size values during the LGM (Fig. 5). Mean grain-size is highest during the latter half of H2 in this record; at 24.25–23.25 ka BP and at the onset of H1. By the Holocene, the mean grain-size does not show great fluctuations, it remains between 8.92 and 29.

Three distinct end-members (EM1–3) from the model were chosen based on the goodness of fit statistics represented by the coefficients of determination and have clearly defined sediment distributions. The two-end-member model showed low r^2 (0.6) for the size range 11–30 μm. The three-end-member model (r^2 mean = 0.82) showed high r^2 (>0.8) for the size spectrum except >110 μm. The four-end-member model showed high r^2 (>0.86) for all size classes except the very fine range (<0.7 and >110 μm). Therefore the goodness of fit statistics demonstrates that the three-end-member model formed the best choice between the number of end-members and r^2. The end-members compare particularly well with those reconstructed from this region (Holz et al., 2004; Tjallingii et al., 2008; Meyer et al., 2013) and corroborate well with modern day dust from the area (Stuut et al., 2005). Therefore, in association with these studies, we infer the finest grained end-member (EM1) as fluvial clay and the two coarser end-members

as fine (EM2) and coarse (EM3) aeolian dust respectively. Within the GeoB7926 record, fluvial and aeolian components demonstrate rapid and large magnitude changes over the last 35 ka BP (Fig. 5). Generally, low amounts of fluvial input occurred except during the B-A and the Holocene (reaching 0.85 at 13.5 and 5 ka BP respectively). Aeolian input was persistent throughout the record with the coarsest material exhibiting relatively high amounts during late MIS3 and the LGM and the finer dust dominating the size fractions during late MIS3 and the YD.

5. Discussion

The multi-proxy analyses performed provide a high resolution reconstruction of palaeoecological, -oceanographic and -climatic variations of the subtropical NE Atlantic since late MIS3. The changes in primary and export productivity with benthic–pelagic coupling in a fundamental upwelling system are detailed here. The benthic foraminifera record of this study is divided into four main intervals corresponding to fundamental climatic events. We discuss the changes in faunal composition of each assemblage, organised according to selected time intervals of the productivity changes, incorporating Late MIS3 (35–28 ka BP), the onset of MIS2; H2 and the LGM (GS-2.1; 28–19 ka BP), H1 (18–15.5 ka BP), B-A (GI-1; 15.5–13.5 ka BP) and the YD (GS-1; 13.5–11.5 ka BP) and finally, the Holocene (11.5–0 ka BP).

Strong coupling occurs during high phytodetritus input and increased upwelling intensity. The highly diversified community of diatoms is indicative of changing hydrographic and oceanographic conditions and productivity regimes over the last 35 ka BP (Fig. 4); see also Romero et al. (2008). When this work is compared to other studies from this particular upwelling region, it becomes apparent that substantial variations in primary productivity occur within a locally confined area as summarised in Table 4. However, an interaction of larger scale atmospheric and oceanographic changes, opposed to just regional change, particularly during Heinrich events, plays an influential role upon the benthos. To summarise our results, a table highlighting our main findings and interpretations is presented (Table 5).

Table 4
Synthesis of a regional perspective of previous findings concerning palaeoproductivity, processes and mechanisms.

Covered time interval	Core	Coordinates	Productivity conditions	Mechanisms	Reference
Late MIS 3	ODP658C, GeoB7920-2	20°45′N, 18°35′W 20°45′N, 18°35′W		Increase wind strength, increase aridity, intense upwelling	Haslett and Smart (2006) Tjallingii et al. (2008) Kohn et al. (2011)
H2	GeoB9527-5	12°26′N, 18°03′W	High foraminiferal production	North Atlantic meltwater events, southerly position of ITCZ, increased wind intensity	Zarriess and Mackensen (2010)
LGM	GeoB5540-2, M13229	27°32′N, 14°10′W 25°10′N	Enhanced foraminiferal and Diatomaceous production	ITCZ expanded north, weaker Trade winds Unfavourable upwelling	Eberwein and Mackensen (2008) Abrantes (2000)
	11K ODP658C GeoB9526-5 GeoB5546-2	21°28′N, 17°57′W 20°45′N, 18°35′W 12°26′N, 18°03′W 27°32′N, 13°44′W	Lower foraminiferal production foraminiferal production Low productivity	Filament formation	Martinez et al. (1999); Zhao et al. (2000) Zarriess and Mackensen (2010) Holzwarth et al. (2010)
H1	GeoB9527-5	12°26′N, 18°13′W	High primary productivity	North Atlantic meltwater events, southerly position of ITCZ, increased wind intensity	Zarriess and Mackensen (2010)
	GeoB 9508-5	15°29′N, 17°57′W	Low to high productivity pattern		Bouimetarhan et al. (2013)
BA	MD03-2705	18°05′N, 21°09′W	High surface productivity	Expanded upwelling area due to active mesoscale dynamics: eddies or low stratification Humid climate, ITCZ moves north.	Matsuzaki et al. (2011)
YD	ODP685C	20°45′N, 18°35′W	Low productivity	Weak upwelling	Haslett and Smart (2006)
Holocene	GeoB5546-2	27°32′N, 13°44′W	Enhanced productivity	ITCZ expanded, intensified African monsoon Late Holocene: increased aridity	Holzwarth et al. (2010)

Table 5
Summary of pelagic—benthic productivity coupling over time and according regional and climatic events.

Assemblage phase	Climatic period	Age (ka BP)	Primary productivity	Dominant benthic fauna	Benthic ecological significance	Synthesis	Reference
1	Late MIS 3	35—28	High	*C. bradyi*	Fresh phytodetritus input, high OM input	Strong benthic-pelagic coupling	Personal comm. Seidenkrantz, M-S & Austin, W.
				N. iridea	High phytodetritus input, high productivity at the sea floor	Strong benthic—pelagic coupling	Polovodova Asteman et al. (2013)
2	H2	25—24	Low to high surficial productivity pattern, comparatively lower	*C. laevigata*	Oxygen poor environment		Murray (1991)
				M. barleeanum	Refractory organic matter in altered form tolerates moderate oxygen depletion		Caralp (1989)
						Tight benthic—pelagic coupling with regards to diatom and benthic foraminiferal flux	Sen Gupta and Machain-Castillo (1993)
	LGM	23—19	Progressive increase in diatom flux	*N. iridea*	High productivity at the sea floor		Gooday and Hughes (2002)
				C. laevigata	High organic input		Corliss and Emerson (1990)
3	H1	18—15.5	Exceptionally high	*E. exilis*	Labile OM input, low oxygen conditions	High surficial productivity hinders benthic diversity & flux	Caralp (1989)
				M. barleeanum	Refractory organic matter in altered form		Caralp (1989)
	BA	15.5—13.5	Moderate-high	*E. exilis*	Labile OM input, low oxygen conditions	Inverse relationship between surface productivity and benthic productivity and diversity	Caralp (1989)
				C. laevigata	Oxygen poor environment		Murray (1991)
				M. pompilioides	Organic rich environment		Fariduddin and Loubere (1997)
				C. wuellerstorfi	Prefer well oxygenated deep-and bottom water conditions		Mackensen et al. (1995), Schmiedl et al. (1997)
	YD	13.5—11.5	Exceptionally high	*E. exilis*	Labile OM input, low oxygen conditions	Still coupled but negative impact on the benthos due to exceptionally high OM input	Caralp (1989)
				G. turgida	Low oxygen, degraded OM		Sweetman et al. (2009)
4	Holocene	11.5—0	Low	*M. barleeanum*	Refractory organic matter in altered form		Caralp (1989)
				M. pompilioides	Organic rich environment		Fariduddin and Loubere (1997)
				C. wuellerstorfi	Oxygenated	Pelagic-benthic decoupling	Lohmann (1978)
				U. peregrina	High organic matter rain rates low to moderate oxygen depletion in the bottom and pore water		Sen Gupta and Machain-Castillo (1993) Schmiedl et al. (1997)

5.1. Assemblage 1: late MIS3 (35–28 ka BP) intense upwelling, high aridity and moderate-to-high benthic–pelagic coupling

Although NW Africa was punctuated by millennial scale humid phases during MIS3 (Holzwarth et al., 2010), late MIS3 was characterised by dry conditions (Haslett and Smart, 2006; Weldeab et al., 2007; Tjallingii et al., 2008). With regard to productivity, this period does not appear stable over time and great fluctuations are recorded in relatively high organic carbon and diatom production, potentially reflecting these rapid climatic switches. Indeed, during 35–28 ka BP, our end-member modelling indicates elevated amounts of fine dust input from the adjacent land mass, via increased wind strength as evidenced from the Ti/Ca values. Our results are consistent with previous studies located along the NW African coast (Zhao et al., 2000) and in particular a low humidity index has been noted for this specific area during MIS3 (Tjallingii et al., 2008; Fig. 6). We propose that increased wind and according upwelling intensity and enhanced surface water production was potentially caused by a change in the wind trajectories.

Our study reveals that the benthic foraminiferal species *C. bradyi* dominated the benthic assemblage during late MIS3 (Fig. 4 and Table 2), with *N. iridea* and *G. crassa* being important accessory species; all of which have an affinity for phytodetritus (Suhr and Pond, 2006; Polovodova Asteman et al., 2013). This applies to H3 also, however, in general, relative increases in benthic foraminifera

concentration and Shannon diversity values occur during decreased diatom concentration over late MIS3 (Figs. 4 and 6). Although modest, this inverse relationship is also apparent from the DAR and BFAR (Fig. 4) and suggests that high primary productivity potentially decreased the BFAR. However, from the benthic faunal composition, we do not find evidence to suggest anoxic conditions at the sea floor, particularly as diversity does not decline. The close correspondence between increased Ti/Ca values and fine dust input, relatively high DAR, abundance of diatom species indicative of high upwelling intensity (Fig. 3; mainly *C. affinis* and *C. diadema* spores) and phytodetritus consuming benthic foraminifera (*C. bradyi*, *N. iridea* and *G. crassa*) indicate that the upwelling conditions provoked a relatively strong pelagic–benthic coupling. From this, we can deduce that the benthic foraminifera responded to productivity at both community scale and at species level (Table 5).

Finally, the BEST statistics suggest that diatoms, TOC, K and Sr explain the benthic foraminiferal faunal composition (Table 3). Potassium is frequently used as indicators of terrigenous supply to the marine environment (Fütterer, 2000) and strontium is very mobile during weathering processes (Meyer et al., 2011). We therefore interpret the benthic faunal changes as a result of higher primary productivity from an increase in nutrient input at the surface water column to be due to high upwelling intensity and weathering processes. We suggest that the upwelling conditions
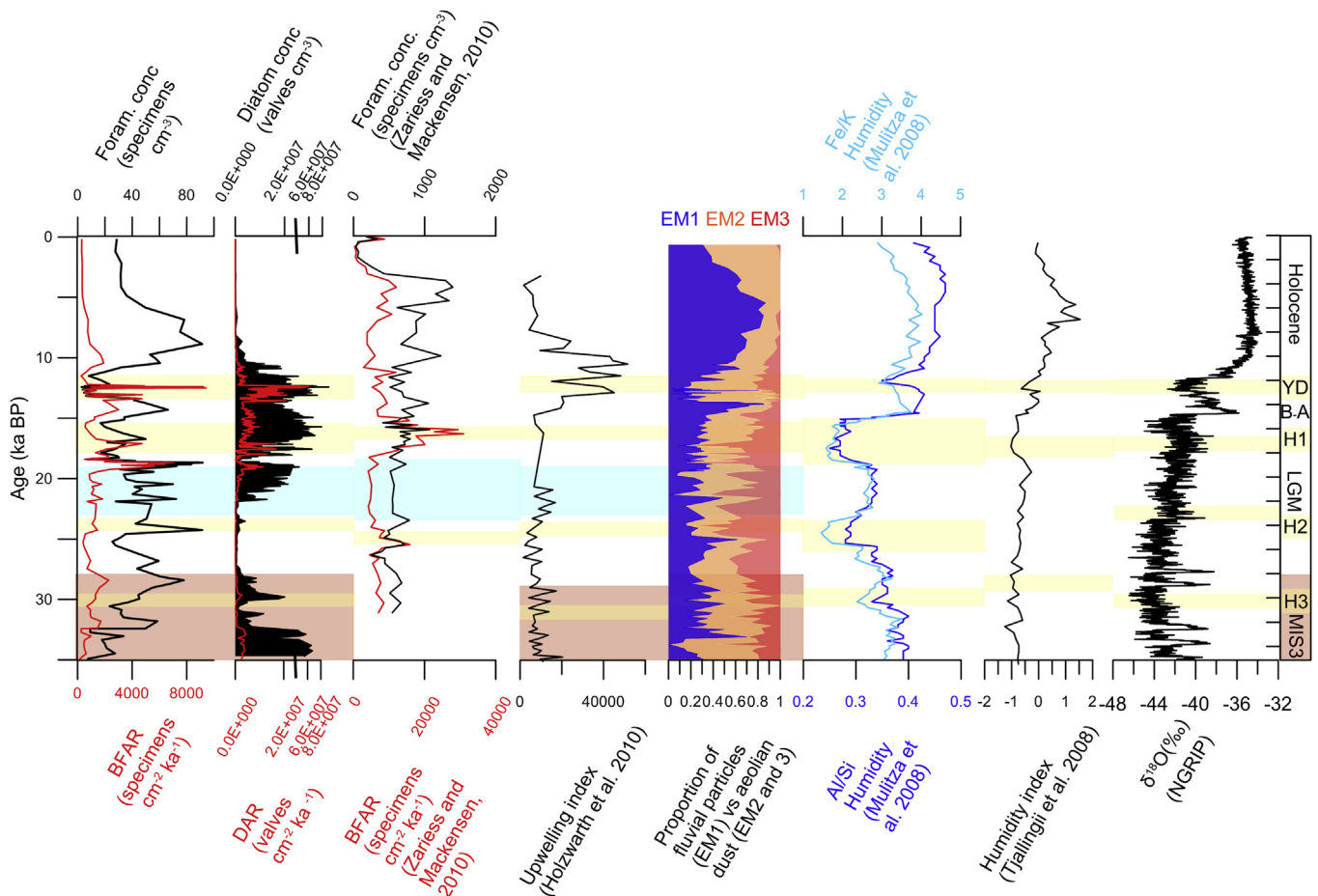

Fig. 6. Palaeoenvironmental records of core GeoB7926, alongside other subtropical NE Atlantic records and the NGRIP ice core (NGRIP Members, 2004) with the Greenland ice core chronology 2005 (GICC05) timescale (Svensson et al. 2008) for the last 35 ka BP. Note that 50 yr were subtracted from the original GICC05 timescale (before yr AD 2000) in order to be comparable with the ^{14}C calibrated time scale. For each individual record, yellow bars indicate the approximate occurence of Heinrich events and also the YD (GS-1). Light blue bars indicate the LGM (GS-2.1). (For interpretation of the references to colour in this figure legend, the reader is referred to the web version of this article.)

and filament locality were optimal for the benthos during MIS3 to support a strong relationship between the pelagic and environment. However, we have not recorded any faunal indications of low oxygen conditions at the sea floor during MIS3.

5.2. Assemblage 2: onset of MIS2; H2 and the LGM (GS-2.1) (28–19 ka BP) fluctuations in upwelling intensity and strong benthic–pelagic coupling

A second benthic foraminiferal shift occurs during 28 to 19 ka BP; incorporating H2 and the LGM. Our results show comparably lower primary productivity and lower BFAR (Fig. 4) with a faunal assemblage showing variable food availability. From 28 to 24 ka BP, the factor analysis of the foraminifera species highlights *G. crassa*, *C. laevigata* and *M. barleeanum*, as being the most significant species (Fig. 4). The former consumes fresh phytoplankton material (Suhr and Pond, 2006) whereas the latter two foraminifera species along with *U. peregrina* consume organic matter of altered form (Caralp, 1989; Schmiedl and Mackensen, 1997), all increase in abundance, albeit not simultaneously. This corresponds with low diatom concentrations until the onset of H2 at 24.5 ka BP. This highlights changes in nutrition obtainability. One plausible explanation is that this refractory material was already present and therefore these species survived on organic matter with low nutritional value (Jorissen and Wittling, 1999). We suggest that upwelling conditions during this time until mid H2 were much weaker, inferred from the Ti/Ca values (Fig. 5) and decline in the abundance of diatoms indicative of strong upwelling (Fig. 3) and therefore not suitable to sustain markedly high export production.

H2 in this study can be regarded as a period allocated into two discrete stages that progressed from an interval of low marine primary productivity from 24.25 to 23.75 ka BP to a phase with higher productivity between 23.75 and 23.25 ka BP. The factor analysis highlights phytodetritus consumers *N. iridea* and *G. crassa* as the main associated species in factor 1 which can be attributed to this assemblage. From this observation, we infer that these two species respond at great rapidity to increasing fresh phytodetritus input and therefore exhibits strong coupling during H2.

During the latter part of H2 (at 23.75–23.25 ka BP), aeolian proxies provide evidence for increased wind intensity and enhanced upwelling which promoted diatom abundance (Fig. 5). This episode coincides with a foraminiferal faunal assemblage that reverts back to a dominance of phytodetritus feeders with the increase in abundance of *N. iridea* and an initial appearance and increase in low oxygen tolerant *E. exilis* at the end of H2 (Fig. 3). We propose the reduction in Atlantic meridional circulation (AMOC) may have contributed to this peak in *E. exilis* by reducing the ventilation and hence dissolved oxygen concentration at lower latitudes. This combined with the increase in diatom abundance (Fig. 4) may have exceeded a threshold as to reduce the foraminiferal abundance and impact the benthic environment to the point of anoxic conditions.

The BEST statistics suggest that this benthic foraminiferal faunal response is caused by the opal and K fluctuations, however, this BEST result is not statistically significant, most likely due to so few samples ($n = 4$) derived from H2. We attribute this primary productivity shift as a result of a significant intensification of the NE trade winds over this region, resulting in strengthened upwelling which in turn promoted nutrient rich sea surface conditions. Abrupt changes in wind intensity and aridity that occur simultaneously with cold high latitude Heinrich ice rafting events have previously been attributed to a southward ITCZ migration (Street-Perrott and Perrott, 1990). This highlights the complexity of the hydrographical setting off the coast of Mauritania and how

atmospheric changes impacts upon upwelling activity and according food availability whereby the benthos responds at great rapidity.

5.2.1. The LGM

At the onset of the LGM at 23 ka BP, the turbidite occurrence (Meggers et al., 2003) and appearance of species such as *Elphidium macellum*; a shallow water, epiphytic species indicate downslope transportation. Recurrent turbidite events occur in this region (Hanebuth and Henrich, 2009) therefore the initial great increase in foraminifera productivity at 22.3–22.9 ka BP has not been included in Fig. 4, as is not a true signal of benthic paleoproduction, but rather an effect of transport.

The dominance of *N. iridea*, *C. bradyi*, *G. crassa* and *C. laevigata* demonstrate high organic input. Again, the species with a preference for fresh phytodetritus demonstrate an instantaneous response to the increase in diatoms (Fig. 4). This emphasises a tight pelagic–benthic connection during the LGM. Our diatom concentrations and DAR demonstrate a progressive increase in pelagic productivity during the LGM (Figs. 4 and 6). As this trend corresponds to relatively moderate BFAR, this again highlights how high organic input can constrain the benthos with regards to population and diversity. In general, from the coarse grain size fraction and diatom group indicative of strong upwelling (Figs. 3 and 5), we infer comparably strong winds and moderately enhanced upwelling intensity.

Our findings are characteristic of other archives from along the NW African coast which have been interpreted as being related to changes in wind intensity (Matsuzaki et al., 2011; Moreno, 2012) and are explained in terms of a southward shift in the ITCZ. In contrast, some sedimentological studies of the NW coast of Africa have shown comparatively weaker trade wind intensity and lower productivity of the subtropical NE Atlantic during the LGM (Zhao et al., 2000; Henderiks and Bollman, 2004; Zarriess and Mackensen, 2010). These contrasting results highlight that palaeoproductivity patterns during the LGM were rather complex and exhibited a spatial heterogeneous response, since the records are all recovered from the same EBCS. These observations emphasise the importance of the proximity to the ITCZ and its according impact upon the trade winds.

The progressive productivity trend could potentially be related to lower sea level during the LGM leading to partly exposing the shelf and different coastal morphology (Holzwarth et al., 2010). This is likely to have resulted in an offshore migration of the upwelling filament and its geometry (Zhao et al., 2000). This movement in the high productivity zone has previously been reported in the NW African upwelling system during the LGM (Giraud and Paul, 2010). Furthermore, as previously postulated by Romero et al. (2008), this comparatively moderate-high primary productivity may be mainly due to upwelling of NACW supplying silica poor water. As this site is situated at the convergence between two upwelling components; the NACW and SACW and the periphery of which migrates in position (Mittelstaedt, 1991; Helmke et al., 2005), we interpret the productivity results to be due to oceanographic and wind regime change. Overall, in spite of stronger trade wind intensity during the LGM, site GeoB7926 demonstrates that global atmosphere-ocean changes lead to localised factors which impact upon the surface productivity and corresponding benthic environmental response.

On a final note, coupling between the near surface environment and the benthos is also reported from the BEST statistical analysis (Table 3), as TOC, biogenic opal and Ti support this notion that organic input, sea surface productivity and upwelling intensity are the influential factors on the benthic fauna, confirming a strong pelagic–benthic interrelationship during the LGM.

5.3. Assemblage 3: H1 (18–15.5 ka BP), B-A (GI-1; 15.5–13.5 ka BP) and the YD (GS-1; 13.5–11.5 ka BP) deglaciation, increased upwelling intensity, high surface productivity and suppressed benthic production

Overall, assemblage 3 is characterised by a great regime shift, both primary productivity and the structure of the benthic foraminiferal fauna change significantly. Now dominated by E. exilis, as confirmed by factor 2 of the factor analysis, the assemblage shows comparably low, although fluctuating, diversity. Overall, during the deglaciation a strong response from the benthos to the export production occurs, as the extremely high DAR promotes low BFAR.

5.3.1. Heinrich event 1

Overall, based on our diatom record, H1 exhibits comparably high primary productivity. Fluctuations in DAR are recorded, with prominent diatom species indicative of strong upwelling across H1. From the increase in the coarse fraction (Fig. 5) during 17–15.5 ka BP we infer increased wind strength, which compares well with the timing of an intensification of the NE trade winds (Bouimetarhan et al., 2013). In particular, it has also been proposed that particularly after 17 ka BP a northward displacement of the Canary Current occurred, potentially due to the AMOC slowdown during H1 (Romero et al., 2008; Gallego-Torres et al., 2014). Therefore, this may have promoted SACW as the main upwelling component, providing silica rich water, shown here by the increased biogenic opal content. Our statistical analysis (Table 3) confirms that opal is the most influential factor upon foraminifera assemblage composition, which supports this notion. This linear relationship between high latitude events, resultant AMOC slowdown and low latitude climate has previously been documented due to the interrelationship with the ITCZ position (Mulitza et al., 2008).

Simultaneously, at ca 17 ka BP, extremely high abundance of the low oxygen tolerant species E. exilis occurs in correspondence to a significant increase in primary productivity as demonstrated by the opal and TOC content (refer to Figs. 4 and 5). This particular species is known to occur in oxygen-poor abyssal waters in this region (Caralp, 1989; Sen Gupta and Machain-Castillo, 1993) and therefore highlights a tight pelagic–benthic coupling (Table 5) to the extent that surface productivity actually has a negative impact on the benthos by promoting hypoxic or possible anoxic conditions. Filipsson et al. (2011) previously reported that low oxygen conditions during the YD were likely due to such large supply of organic matter and fresh phytodetritus to the seafloor that caused a reduction in pore water oxygen content during remineralisation (Jahnke et al., 1994). Of integral significance is the almost complete decline of C. bradyi and G. crassa which rely on the same fresh phytoplankton diet (Suhr and Pond, 2006) in conjunction with the instantaneous thriving of E. exilis. This provides substantial evidence that the benthic oxygenation levels crossed a threshold whereby the former species could no longer survive. Furthermore, benthic foraminifera concentrations are relatively low during H1 (Fig. 6). These observations confirm that food supply derived from surface primary productivity and oxygen levels are the principal influence on the benthic foraminifera assemblages within this upwelling system. In recent studies, considerable emphasis has been placed on these limiting factors (Gooday, 2003). Our study explicitly provides evidence that organic export and oxygen are the two key factors governing the benthic foraminiferal community composition.

Paradoxically, observations made southward at 12°N have demonstrated high benthic foraminiferal concentrations (Zarriess and Mackensen, 2010) as shown in Fig. 6. More specifically, their record showed no evidence of E. exilis abundance but low organic carbon input. This was interpreted in terms of an offshore migration of the upwelling cell. Such contrasting results could be due to the latitude of the core site and associated position of the ITCZ.

All of these proxies converge to imply enhanced productivity related to an increase nutrient input and strengthened upwelling system during the latter phase of H1 (17–15.5 ka BP), which caused benthic foraminifera diversity to be low and the assemblage to be indicative of low oxygen conditions. The BEST statistics (Table 3) suggest that opal, Ti, K and Sr represent the most influential environmental factors upon the benthic foraminiferal faunal assemblages. This supports our interpretations that nutrient enhanced upwelled waters and stronger winds promoted upwelling conditions suitable for such high diatom abundance which provided excessive phytodetritus input to the benthos.

5.3.2. Bølling-Allerød (GI-1)

The Bølling-Allerød (B-A) period is characterised by low Ti/Ca values and grain size with a dominance of the fluvial end-member component of the terrigenous input (Filipsson et al., 2011) which points to lower wind and according upwelling intensity and humid conditions. Despite the fact that there is currently no fluvial activity in the vicinity of site GeoB7926, a palaeo river system is evident from topographical studies (Vörösmarty et al., 2000) could potentially have been an active source during humid events. This African Humid Period is well documented and has been attributed to a strengthening of the African monsoon (deMenocal et al., 2000b). A diverse range of proxy data highlight a prompt onset of a humid climate during the B-A which corresponds with our record. Lake level and pollen studies from the West Africa region suggest higher precipitation and an increased abundance of temperate taxa (Hoelzmann et al., 1998). Furthermore, this climatic shift has also been registered in elemental records from 15°N whereby Al/Si and Fe/K values correlate well with our end-member results (Mulitza et al., 2008; Fig. 6).

Our results provide evidence of comparatively high surface productivity, albeit not as extensive as H1. This occurs in conjunction with a decreased abundance of E. exilis relative to H1 and YD (Fig. 4, Table 5) and other species increase in abundance, such as C. wuellerstorfi, a species which requires oxygenated conditions (e.g. Schmiedl et al., 1997) and U. peregrina. We therefore suggest that the benthic environment returned to more oxygenated conditions during the B-A with adequate organic contribution. The BEST statistics suggest TOC as the main controlling factor upon the benthic foraminiferal assemblage highlighting again the coupling with pelagic organic input. Altogether, these observations suggest that the upwelling conditions, primary productivity and subsequent organic matter input were at a suitable level for the benthic foraminifera to recover in diversity after the low oxygen conditions that occurred previously during H1.

5.3.3. Younger Dryas (GS-1)

During YD, enhanced Ti/Ca values, increased mean grain-size and high DAR and diatom concentrations are clearly evidenced (Figs. 4 and 6). From this we deduce that the YD period exhibits a rapid intensification of the trade wind and upwelling. This agrees well with other records, for example the upwelling index of Holzwarth et al. (2010) from a study conducted further north at 27°N (Fig. 6). Furthermore, high biogenic opal maxima during each glacial termination over longer timescales have been reported from the NW Africa upwelling system (Meckler et al., 2013). These peaks in opal export have been found to be consistent with a reduced formation of silica depleted glacial North Atlantic intermediate water (GNAIW) (McManus et al., 2004) which has been proposed to encourage mixing and the ascendancy of silica-rich deep water to the surface ocean at low latitudes.

The high diatom productivity provoked by intense upwelling activity in the GeoB7926 record is coupled with low foraminifera concentrations and diversity. However, whilst DAR is high, spores indicating strong upwelling decline during the YD as diatoms

representing lower productivity increase (Fig. 3). One hypothesis of the underlying reason for this contrasting signal in diatom indicators is the ballasting effect. Iversen et al. (2010) suggest that diatom concentrations are important predecessors for aggregate formation which exports organic matter to the sea floor and that high aeolian dust flux results in increased export off Mauritania via ballasting. We propose that diatoms and other primary producers are drawn down from the surface ocean via this process. Therefore, regardless of the increased upwelling intensity providing nutrient rich waters, the diatom species may not be representative of the surface conditions at site GeoB7926 due to export of organic matter to the benthos at an increased sinking velocity of aggregates formed from high fine grained dust input (Fig. 5). This exceedingly high export demonstrates a pronounced disadvantage of the benthic community during the YD (Filipsson et al., 2011).

Over the course of the YD, the benthic foraminiferal assemblage composed almost entirely of low oxygen tolerant taxa *E. exilis* and *Globobulimina turgida* (Table 5) which suggests a return to low oxygen conditions at the sea floor. As the Shannon diversity is so low due to the majority of other species being almost in complete decline. One plausible explanation is that the ocean bottom water conditions turned hypoxic during the YD. We define the persistence and increase abundance of the low oxygen tolerant *E. exilis* as a degree of oxygen depletion which has induced stress on the rest of the community (Tyson and Pearson, 1991). Moreover, this emphasises the role of food input and oxygen as the two foremost controlling factors that impact the benthos. Overall, the YD benthic foraminiferal community composition shows a response to changes in hydrography and climatic conditions. Furthermore, the BEST statistical analyses show that the redox sensitive element Mn corresponds with this faunal change, emphasising low oxygen conditions. This is further supported by bulk geochemistry data of GeoB7926 (Gallego-Torres et al., 2014) whereby water column anoxia and deep water ventilation from AMOC slowdown have been evidenced from Mo enrichment, enhanced by high export productivity.

5.4. Assemblage 4: the Holocene (11.5–0 ka BP) decreased upwelling intensity and low pelagic and benthic productivity

Holocene climate is recognised by significant productivity and environmental changes with a fourth shift in the benthic foraminiferal assemblage at 11 ka BP.

Diatom species such as *Actinocyclus senarius* which thrive in warm waters (Romero et al., 2008) characterise the Holocene (Fig. 3), with DAR much lower than previously recorded in GeoB7926-2. This therefore suggests the establishment of low productive conditions over the area however; it is widely known that the Holocene is not a period of constantly warm climatic conditions (deMenocal et al., 2000b) and our record is no exception. With regards to upwelling intensity, we interpret the diatom record as indicative of comparably weaker upwelling.

By observing our end-member model results, we can consider that high fluvial inputs reflect periods of increase humidity over the adjacent continent, particularly during the early Holocene. This is supported by other studies from this region whereby dust transport declined as a result of weaker wind intensities (e.g. Mulitza et al., 2008; Fig. 6). In the early Holocene, also termed the "African humid period" (deMenocal et al., 2000b), the climatic conditions of the NW African region were significantly different, whereby the adjacent land mass was more humid due to the monsoonal system (Gasse, 2000) and weaker intensity of the trade winds (Kuhlmann et al., 2004).

Subsequently, at ca 9 ka BP (late Holocene), the sharp increase from low to high Ti/Ca ratios in tandem with a shift to a dominance of fine aeolian sediment opposed to the previous recurrent fluvially derived fine particles (Fig. 5) indicates more arid conditions. This mid

Holocene shift to arid conditions is in accordance with other studies of NW Africa climate (Sarnthein et al., 1982; Gasse, 2002; Meyer et al., 2013). Rapid climate changes during the interval 8.5 ka BP have previously been reported in the African subtropics and attributed to coincide with the most prominent Holocene climate event at high latitudes, observed in Greenland ice-cores (Alley et al., 1997). This is interpreted as a transfer to present arid conditions occurring now in NW Africa. Whilst diatom productivity did not exhibit a response to this transition, we show here that the benthic foraminifera concentration, BFAR and CaCO$_3$ also exhibit high values during the early Holocene before rapidly declining in the latter half of this climatic period. The striking increase in CaCO$_3$ over the first half of the Holocene suggests a dominance of calcareous producers. Overall, the Holocene reveals a final, marked structural shift in the benthic foraminiferal faunal composition and diversity within the GeoB7926-2 record (Figs. 4 and 6) which we hypothesise is associated with changes in atmospheric conditions and reduced upwelling intensity. Moreover, the Shannon diversity values are the highest of this entire record and therefore we interpret that the reduction in export productivity allows oxygen levels at the seafloor to recover which in turn, enables the establishment of a diverse benthic community. This is supported by the rapid decrease in *E. exilis* and an increased presence of *C. wuellerstorfi*. In addition, the Holocene sees *U. peregrina* thriving and a return of *M. barleeanum* and other species that have preference for a more refractory organic matter diet, which highlights organic material of altered form being more readily available than fresh phytodetritus.

Therefore, we can thus consider that the corresponding high fluvial input provided an alternative food source to the benthos. In addition, the BEST statistical analysis show the factors explaining the foraminifera abundance changes through the Holocene are mean grain-size and opal, both of which are low during the Holocene. As diatoms are the highest contributor to opal content in core GeoB7926 (with other siliceous components providing low contributions), we interpret the BEST result to suggest a decoupling between the pelagic and benthic environment due to lower upwelling intensity and accordingly, lower surface production. Overall, we demonstrate that the Holocene should not be regarded as an interval of merely comparatively low surface productivity conditions, but also a period divided into contrasting hydrological and benthic productivity phases.

6. Conclusion

The high resolution, multi-proxy study analysed here provides new insights regarding millennial scale palaeoproductivity changes over the last 35 ka BP in the subtropical NE Atlantic. Pelagic and benthic productivity fluctuations at site GeoB7926 suggest a strong connection with subtropical climate change at well as high latitudinal variations through the shifting in position of the ITCZ and ocean circulation changes.

This study highlights that substantial ecological interrelationships are governed by a complex, interchanging set of factors, namely upwelling intensity, nutrient source and hydrographic conditions. Four benthic foraminiferal assemblages are present in the GeoB7926 record corresponding to fundamental high latitude climatic events, firstly during late MIS3, secondly during early MIS2, H2 and the LGM, thirdly from H1 to the YD and finally over the Holocene. The changes in benthic foraminifera community composition reveal rapid responses to changes in primary and export productivity regimes as well as bottom water conditions. In particular, we show explicitly that oxygen and food are the utmost important factors controlling benthic foraminiferal assemblages.

Arid climate conditions on the NW African continent prevailed during late MIS3, H2, LGM, H1 and YD and humid conditions arose

during B-A and the Early Holocene. MIS3, H2 and the LGM are characterised by moderate surface productivity and both the benthic productivity and community composition showed tight pelagic– benthic coupling. Our data shows prominent coupling between the sea surface and bottom waters during periods of high phytodetritus input, particularly during H1 and YD where such exceedingly high primary production led to detrimental effects at the sea floor by promoting low oxygen conditions, illustrated by the dominance of *E. exilis.* The Holocene is defined as a comparatively more stable and lowered productivity period with regards to primary production and benthic foraminiferal abundance with atmospheric and hydrological changes of large amplitude potentially having a more dominant effect on the benthic foraminiferal concentrations. By comparing our data with different records from this region, we validate our findings as well as highlight variations in primary and export production within a locally confined area. This emphasises the impact of not only upwelling intensity but also filament position and extension upon the underlying benthic environment.
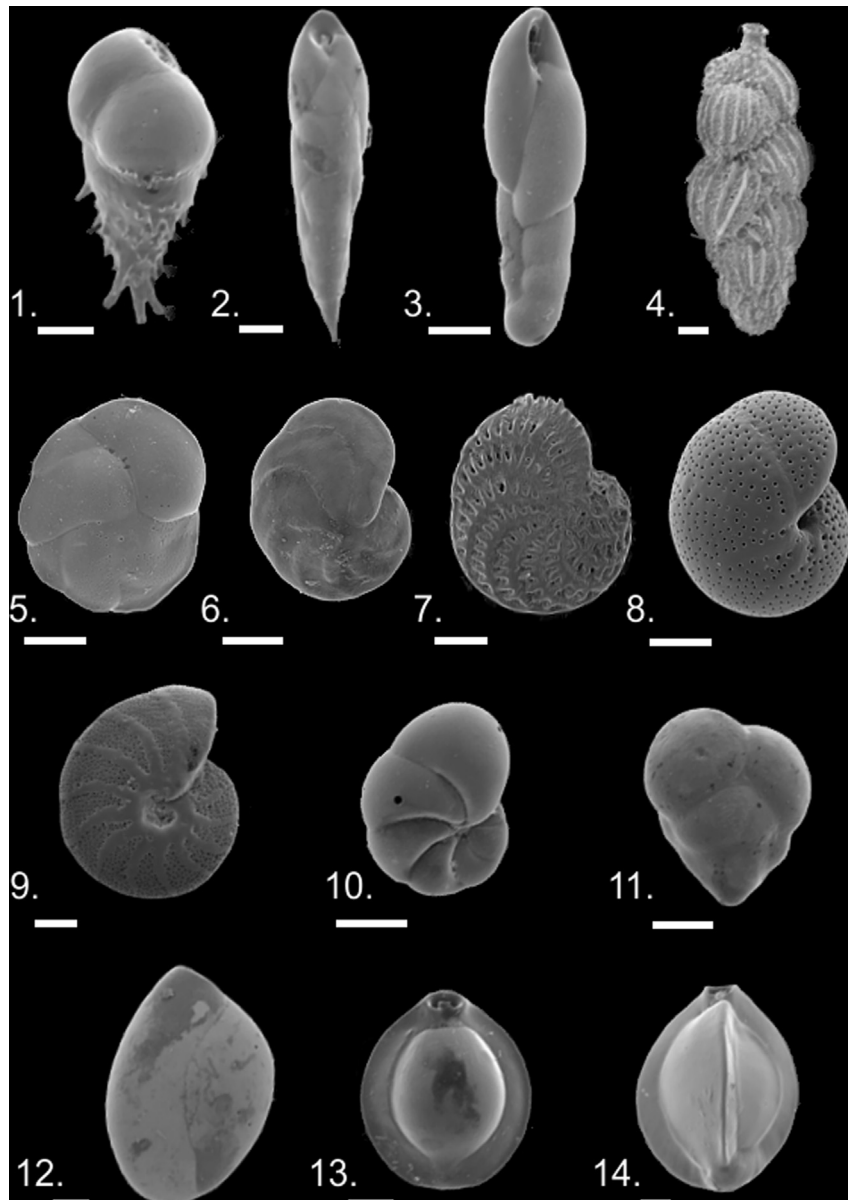
Acknowledgements

Appendix

Plate 1.

1. *Bulimina aculeata* d'Orbigny, 1826
2. *Eubuliminella exilis* (Brady, 1884)
3. *Cassidella bradyi* (Cushman, 1922)
4. *Uvigerina peregrina* Cushman, 1923
5. *Cassidulina laevigata* d'Orbigny 1826
6. *Cibicides wuellerstorfi* (Schwager, 1866)
7. *Elphidium macellum* (Fichtel and Moll, 1798); Knudsen (1973): p. 287, pl. 2, fig. 7.
8. *Melonis pompilioides* (Fichtel and Moll, 1798); Eberwein (2006): p. 103, pl. 2, fig. 3.
9. *Melonis barleeanum* (Williamson, 1858); Eberwein (2006): p 103, pl. 2, fig. 2.
10. *Nonionella iridea* Heron-Allen and Earland, 1932
11. *Tosaia hanzawai* Takayanagi, 1953
12. *Quinqueloculina seminulum* (Linnaeus, 1758); Ingle et al. (1980): p. 142, pl. 9, figs. 14–15.
13. *Pyrgo murrhina* (Schwager, 1866)
14. *Triloculina tricarinata* d'Orbigny, 1826

SEM images of common, recurrent and transported (*E. macellum* and *T. hanzawai*) benthic foraminiferal species in >150 μm fraction within the GeoB7926 record. Each scale bar represents 100 μm.

References

Abrantes, F., 2000. 200 000 yr diatom records from Atlantic upwelling sites reveal maximum productivity during LGM and a shift in phytoplankton community structure at 185 000 yr. Earth Planet. Sci. Lett. 176, 7–16.

Alley, R.B., Mayewski, P.A., Sowers, T., Stuiver, M., Taylor, K.C., Clark, P.U., 1997. Holocene climatic instability: a prominent, wide-spread event 8200 yr ago. Geology 25, 483–486.

Arz, H.W., Pätzold, J., Wefer, G., 1998. Correlated millennial-scale changes in surface hydrography and terrigenous sediment yield inferred from Last-Glacial marine deposits off Northeastern Brazil. Quat. Res. 50, 157–166.

Bard, E., 1988. Correction of accelerator mass spectrometry ^{14}C ages measured in planktonic foraminifera: paleoceanographic implications. Paleoceanography 3, 635–645.

Bouimetarhan, I., Groeneveld, J., Dupont, L., Zonneveld, K., 2013. Low- to high-productivity pattern within Heinrich Stadial 1: inferences from dinoflagellate cyst records off Senegal. Glob. Planet. Change 106, 64–76.

Brady, H.B., 1884. Report on the foraminifera dredged by H.M.S. Challenger during the years 1873-1876, Report of the scientific results of the voyage of H.M.S. Challenger, 1873-1876. Zoology, 1–814.

Caralp, M.H., 1989. Abundance of Bulimina exilis and Melonis barleeanum: relationship to the quality of marine organic matter. Geo-Mar. Lett. 9, 37–43.

Clarke, K.R., Gorley, R.N., 2006. PRIMER v6: User Manual/Tutorial. PRIMER-E, Plymouth.

Corliss, B.H., Emerson, S., 1990. Distribution of Rose Bengal stained benthic foraminifera from the Nova Scotia continental margin and Gulf of Maine. Deep-Sea Res. 37, 381–400.

d'Orbigny, A., 1826. Tableau methodique de la classe des Cephalopodes. Ann. Des. Sci. Nat. Ser. 1, 245–314.

DeMaster, D.J., 1981. The supply and accumulation of silica in the marine environment. Geochim. Cosmochim. Acta 45, 1715–1732.

deMenocal, P., Ortiz, J., Guilderson, T., Adkins, J., Sarnthein, M., Baker, L., Yarusinsky, M., 2000a. Abrupt onset and termination of the African Humid Period: rapid climate responses to gradual insolation forcing. Quat. Sci. Rev. 19, 347–361.

deMenocal, P., Ortiz, J., Guilderson, T., Sarnthein, M., 2000b. Coherent high- and low-latitude climate variability during the Holocene warm period. Science 288, 2198–2202.

Eberwein, A., 2006. Holocene and Last Glacial Maximum (paleo-) Productivity off Morocco: Evidence from Benthic Foraminifera and Stable Carbon Isotopes. Alfred Wegener Institute for Polar and Marine Research, Bremerhaven, pp. 1–103.

Eberwein, A., Mackensen, A., 2008. Last Glacial Maximum paleoproductivity and water masses off NW-Africa: Evidence from benthic foraminifera and stable isotopes. Mar. Micropaleontol 67, 87–103.

Fariduddin, M., Loubere, P., 1997. The surface ocean productivity response of deeper water benthic foraminifera in the Atlantic Ocean. Mar. Micropaleontol. 32, 289–310.

Filipsson, H.L., Romero, O.E., Stuut, J.-B.W., Donner, B., 2011. Relationships between primary productivity and bottom-water oxygenation off northwest Africa during the last deglaciation. J. Quat. Sci. 26, 448–456.

Fütterer, D.K., 1983. The Modern Upwelling record off Northwest Africa. In: Thiede, J., Suess, E. (Eds.), Coastal Upwelling: Its Sediment Record, Part B. Sedimentary Records of Ancient Coastal Upwelling. Plenum Press, London, pp. 105–121.

Fütterer, D.K., 2000. The solid phase of marine sediments. In: Schulz, H.D., Zabel, M. (Eds.), Marine Geochemistry. Springer, New York, pp. 1–22.

Gallego-Torres, D., Romero, O.E., Martnez-Ruiz, F., Kim, J.-H., Donner, B., Ortega-Huertas, M., 2014. Rapid bottom-water circulation changes during the last glacial cycle in the coastal low-latitude NE Atlantic. Quat. Res. 81, 330–338.

Gardener, D., 1977. Nutrients as tracer of water mass structure in the coastal upwelling of Northwest Africa. In: Angel, M. (Ed.), A Voyage of Discovery. Pergamon Press, Oxford.

Gasse, F., 2000. Hydrological changes in the African tropics since the Last Glacial Maximum. Quat. Sci. Rev. 19, 189–211.

Gasse, F., 2002. Diatom-inferred salinity and carbonate oxygen isotopes in Holocene waterbodies of the western Sahara and Sahel (Africa). Quat. Sci. Rev. 21, 737–767.

Giraud, X., Paul, A., 2010. Interpretation of the paleo-primary production record in the NW African coastal upwelling system as potentially biased by sea level change. Paleoceanography 25, PA4224.

Gooday, A.J., 1988. A response by benthic foraminifera to the deposition of phytodetritus in the deep sea. Nature 332, 70–73.

Gooday, A.J., Hughes, J.A., 2002. Foraminifera associated with phytodetritus deposits at a bathyal site in the northern Rockall Trough (NE Atlantic): seasonal contrasts and a comparison of stained and dead assemblages. Mar. Micropaleontol. 46, 83–110.

Gooday, A.J., 2003. Benthic foraminifera (protista) as tools in deep-water palaeoceanography: environmental influences on faunal characteristics. Adv. Mar. Biol., 1–90. Academic Press.

Gooday, A.J., Jorissen, F.J., 2012. Benthic foraminiferal biogeography: controls on global distribution patterns in deep-water settings. Annu. Rev. Mar. Sci. 4, 237–262.

Hagen, E., Zulicke, C., Feistel, R., 1996. Near-surface structures in the Cape Ghir filament off Morocco. Oceanol. Acta 19, 577–598.

Hammer, Ø., Harper, D.A.T., Ryan, P.D., 2001. PAST: paleontological statistics software package for education and data analysis. Palaeontol. Electron. 4, 9.

Hanebuth, T.J.J., Henrich, R., 2009. Recurrent decadal-scale dust events over Holocene western Africa and their control on canyon turbidite activity (Mauritania). Quat. Sci. Rev. 28, 261–270.

Haslett, S.K., Smart, C.W., 2006. Late Quaternary upwelling off tropical NW Africa: new micropalaeontological evidence from ODP Hole 658C. J. Quat. Sci. 21, 259–269.

Helmke, P., Romero, O., Fischer, G., 2005. Northwest African upwelling and its effect on offshore organic carbon export to the deep sea. Glob. Biogeochem. Cycles 19, GB4015.

Henderiks, J., Bollman, J., 2004. The Gephyrocapsa sea surface palaeothermometer put to the test: comparison with alkenone and foraminifera proxies off NW Africa. Mar. Micropaleontol. 50, 161–184.

Heron-Allen, E., Earland, A., 1932. Protozoa, Part II Foraminifera. British Antarctic ("Terra Nova") Expedition, 1910. In: Natural History Reports, Zoology, vol. 6, pp. 25–268.

Hoelzmann, P., Jolly, D., Harrison, S.P., Laarif, F., Bonnefille, R., Pachur, H.J., 1998. Mid-Holocene land-surface conditions in northern Africa and the Arabian Peninsula: a data set for the analysis of biogeophysical feedbacks in the climate system. Glob. Biogeochem. Cycles 12, 35–51.

Holz, C., Stuut, J.-B.W., Henrich, R., 2004. Terrigenous sedimentation processes along the continental margin off NW-Africa: implications from grain-size analyses of surface sediments. Sedimentology 51, 1145–1154.

Holzwarth, U., Meggers, H., Esper, O., Kuhlmann, H., Freudenthal, T., Hensen, C., Zonneveld, K.A.F., 2010. NW African climate variations during the last 47,000 years: evidence from organic-walled dinoflagellate cysts. Palaeogeogr. Palaeoclimatol. Palaeoecol. 291, 443–455.

Ingle Jr., J.C., Keller, G., Kolpack, R.L., 1980. Benthic foraminiferal biofacies, sediments and water masses of the Southern Peru-Chile Trench area, Southeastern Pacific ocean. Micropaleontology 26, 113–150.

Iversen, M.H., Nowald, N., Ploug, H., Jackson, G.A., Fischer, G., 2010. High resolution profiles of vertical particulate organic matter export off Cape Blanc, Mauritania: degradation processes and ballasting effects. Deep Sea Res. Part I Oceanogr. Res. Pap. 57, 771–784.

Jahnke, R.A., Craven, D.B., Gaillard, J.-F., 1994. The influence of organic matter diagenesis on CaCO3 dissolution at the deep-sea floor. Geochim. Cosmochim. Acta 58, 2799–2809.

Jones, R.W., 1994. The Challenger Foraminifera. Oxford University Press, Oxford.

Jorissen, F.J., 1999. Benthic foraminiferal microhabitats below the sediment-water interface. In: Sen Gupta, B.K. (Ed.), Ecology of Recent Foraminifera. Kluwer Academic Publishers, pp. 161–179.

Jorissen, F.J., Wittling, I., 1999. Ecological evidence from live–dead comparisons of benthic foraminiferal faunas off Cape Blanc (Northwest Africa). Palaeogeogr. Palaeoclimatol. Palaeoecol. 149, 151–170.

Jorissen, F.J., Wittling, I., Peypouquet, J.P., Rabouille, C., Relexans, J.C., 1998. Live benthic foraminiferal faunas off Cape Blanc, NW-Africa: community structure and microhabitats. Deep Sea Res. Part I Oceanogr. Res. Pap. 45, 2157–2188.

Kim, J.-H., Meggers, H., Rimbu, N., Lohmann, G., Freudenthal, T., Muller, P.J., Schneider, R.R., 2007. Impacts of the North Atlantic gyre circulation on Holocene climate off northwest Africa. Geology 35, 387–390.

Kim, J.-H., Romero, O.E., Lohmann, G., Donner, B., Laepple, E.H., Jaap, S., Damste, S., 2012. Pronounced subsurface cooling of North Atlantic waters of Northwest Africa during Dansgaard-Oeschger interstadials. Earth Planet. Sci. Lett. 339–340, 95–102.

Knoll, M., Hernández-Guerra, A., Lenz, B., López Laatzen, F., Machín, F., Müller, T.J., Siedler, G., 2002. The eastern boundary current system between the Canary Islands and the African coast. Deep Sea Res. Part II Top. Stud. Oceanogr. 49, 3427–3440.

Knudsen, K.L., 1973. Foraminifera from postglacial deposits of the Lundergård area in Vendsyssel, Denmark. Bull. Geol. Soc. Den. 22, 255–282.

Kohn, M., Steinke, S., Baumann, K.-H., Donner, B., Meggers, H., Zonneveld, K., 2011. Stable oxygen isotopes from the calcareous-walled dinoflagellate Thoracosphaera heimii as a proxy for changes in mixed layer temperatures off NW Africa during the last 45,000 yr. Palaeogeogr. Palaeoclimatol. Palaeoecol. 302, 311–322.

Koopmann, B., 1981. Sedimentation von Saharastaub im sub-tropischen Nordatlantik während der letzen 25.000 Jahre. Meteor Forschungsergebnisse 35, 23–59.

Krastel, S., Hanebuth, T.J.J., Antobreh, A.A., Henrich, R., Holz, C., Kölling, M., Schulz, H.D., Wien, K., Wynn, R.B., 2004. Cap Timiris Canyon: a newly discovered channel system offshore of Mauritania. Eos Trans. Am. Geophys. Union 85, 417–423.

Kuhlmann, H., Meggers, H., Freudenthal, T., Wefer, G., 2004. The transition of the monsoonal and the N Atlantic climate system off NW Africa during the Holocene. Geophys. Res. Lett. 31, L22204.

Loeblich, A.R., Tappan, H., 1987. Foraminiferal Genera and Their Classification. Van Nostrand Reinhold, New York.

Lohmann, G.P., 1978. Abyssal benthonic foraminifera as hydrographic indicators in the western South Atlantic. J. Foraminifer. Res. 8, 6–34.

Lutze, G.F., Coulbourn, W.T., 1983. Recent benthic foraminifera from the continental margin of northwest Africa: community structure and distribution. Mar. Micropaleontol. 8, 361–401.

Mackensen, A., Schmiedl, G., Harloff, J., Giese, M., 1995. Deep-sea Foraminifera in the South Atlantic Ocean: ecology and assemblage generation. Micropaleontology 41, 342–358.

Martinez, P., Bertrand, P., Shimmield, G.B., Karen, C., Jorissen, F.J., Foster, J., Dignan, M., 1999. Upwelling intensity and ocean productivity changes off Cape Blanc (northwest Africa) during the last 70,000 years: geochemical and micropalaeontological evidence. Mar. Geol. 158, 57–74.

Matsuzaki, K.M.R., Eynaud, F., Malaizé, B., Grousset, F.E., Tisserand, A., Rossignol, L., Charlier, K., Jullien, E., 2011. Paleoceanography of the Mauritanian margin during the last two climatic cycles: from planktonic foraminifera to African climate dynamics. Mar. Micropaleontol. 79, 67–79.

McGregor, H.V., Dima, M., Fischer, H.W., Mulitza, S., 2007. Rapid 20th-Century Increase in Coastal Upwelling off Northwest Africa. Science 315, 637–639.

McManus, J.F., Francois, R., Gherardi, J.M., Keigwin, L.D., Brown-Leger, S., 2004. Collapse and rapid resumption of Atlantic meridional circulation linked to deglacial climate changes. Nature 428, 834–837.

Meckler, A.N., Sigman, D.M., Gibson, K.A., Francois, R., Martinez-Garcia, A., Jaccard, S.L., Rohl, U., Peterson, L.C., Tiedemann, R., Haug, G.H., 2013. Deglacial pulses of deep-ocean silicate into the subtropical North Atlantic Ocean. Nature 495, 495–498.

Meggers, H., Babero-Munoz, L., Barrera, C., et al., 2003. Report and Preliminary Results of METEOR Cruise M 53/1, Limassol–Las Palmas–Mindelo, 30.03.–03.05.2002. Berichte aus dem Fachbereich Geowissenschaften der Universität Bremen. Universität Bremen.

Meyer, I., Davies, G.R., Stuut, J.-B.W., 2011. Grain size control on Sr-Nd isotope provenance studies and impact on paleoclimate reconstructions: an example from deep-sea sediments offshore NW Africa. Geochem. Geophys. Geosyst. 12, Q03005.

Meyer, I., Davies, G.R., Vogt, C., Kuhlmann, H., Stuut, J.-B.W., 2013. Changing rainfall patterns in NW Africa since the Younger Dryas. Aeolian Res. 10, 111–123.

Mittelstaedt, E., 1983. The upwelling area off Northwest Africa—A description of phenomena related to coastal upwelling. Prog. Oceanogr. 12, 307–331.

Mittelstaedt, E., 1991. The ocean boundary along the northwest African coast: circulation and oceanographic properties at the sea surface. Prog. Oceanogr. 26, 307–355.

Mittelstaedt, E., Pillsbury, D., Smith, R.L., 1975. Flow patterns in the Northwest African upwelling area. Dtsch. Hydrogr. Z. 28, 145–167.

Moreno, A., 2012. A multiproxy paleoclimate reconstruction over the last 250 kyr from marine sediments: the northwest African margin and the western Mediterranean Sea. In: Hublin, J.J., McPherron, S.P. (Eds.), Modern Origins: a North African Perspective. Springer Science and Business, pp. 3–17.

Mulitza, S., Prange, M., Stuut, J.-B.W., Zabel, M., von Dobeneck, T., Itambi, A.C., Nizou, J., Schulz, M., Wefer, G., 2008. Sahel megadroughts triggered by glacial slowdowns of Atlantic meridional overturning. Paleoceanography 23. http://dx.doi.org/10.1029/2008PA001637.

Müller, P., Schneider, R.R., 1993. An automated leaching method for the determination of opal in sediments and particulate matter. Deep-Sea Res. Part I 40, 425–444.

Murray, J.W., 1991. Ecology and Palaeoecology of Benthic Foraminifera Longman Scientific and Technical. Harlow, UK.

NGRIP Members, 2004. High resolution record of Northern Hemisphere climate extending into the last interglacial period. Nature 431, 147–151.

Nicholson, S.E., 1986. The spatial coherence of African rainfall anomalies: interhemispheric teleconnections. J. Clim. Appl. Meteorol. 25, 1365–1381.

Pelegrí, J.L., Arístegui, J., Cana, L., González-Dávila, M., Hernández-Guerra, A., Hernández-León, S., Marrero-Díaz, A., Montero, M.F., Sangrà, P., Santana-Casiano, M., 2005. Coupling between the open ocean and the coastal upwelling region off northwest Africa: water recirculation and offshore pumping of organic matter. Journal of Marine Systems 54, 3–37.

Polovodova Asteman, I., Nordberg, K., Filipsson, H.L., 2013. The Little Ice Age: evidence from a sediment record in Gullmar Fjord, Swedish west coast. Biogeosciences 10, 1275–1290.

Prospero, J.M., Carlson, T.N., 1981. Saharan air outbreaks over the tropical North Atlantic. PAGEOPH 119, 677–691.

Rasmussen, S.O., Bigler, M., Blockley, S.P.E., Blunier, T., Buchardt, S.L., Clausen, H.B., Cvijanovic, I., Dahl-Jensen, D., Johnsen, S.J., Fischer, H., Gkinis, V., Guillevic, M., Hoek, W.Z., Lowe, J.J., Pedro, J., Popp, T., Seierstad, I.K., Steffensen, J.P., Svensson, A.M., Vallelonga, P., Vinther, B.M., Walker, M.J.C., Wheatley, J.J. and Winstrup, M., A stratigraphic framework for robust naming and correlation of abrupt climatic changes during the last glacial period based on three synchronized Greenland ice core records. Quat. Sci. Rev. in revision.

Reimer, P.J., Baillie, M.G.L., Bard, E., Bayliss, A., Beck, J.W., Blackwell, P.G., Ramsey, C.B., Buck, C.E., Burr, G.S., Edwards, R.L., Friedrich, M., Grootes, P.M., Guilderson, T.P., Hajdas, I., Heaton, T.J., Hogg, A.G., Hughen, K.A., Kaiser, K.F., Kromer, B., McCormac, F.G., Manning, S.W., Reimer, R.W., Richards, D.A., Southon, J.R., Talamo, S., Turney, C.S.M., van der Plicht, J., Weyhenmeyer, C.E., 2009. IntCal09 and Marine09 radiocarbon age calibration curves, 0-50,000 years cal BP. Radiocarbon 51, 1111–1150.

Romero, O.E., Kim, J.-H., Donner, B., 2008. Submillennial-to-millennial variability of diatom production off Mauritania, NW Africa, during the last glacial cycle. Paleoceanography 23. http://dx.doi.org/10.1029/2008PA001601.

Sarnthein, M., Thiede, J., Pflaumann, U., Erlenkeuser, H., Fütterer, D., Koopman, b., Lange, H., Seibold, E., 1982. Atmospheric and oceanic circulation patterns off northwest Africa during the past 25 million years. In: von Rad, U. (Ed.), Geology of Northwest African Continental Margin. Springer, Berlin, pp. 545–604.

Schemainda, R., Nehring, D., Schultz, S., 1975. Ozeanologische Untersuchungen zum Produktionspotential der nordwestafrikanischen Wasserauftriebsregion 1970-1973. Geod. geophys. Veröff. 4, 85.

Schmiedl, G., Mackensen, A., 1997. Late Quaternary paleoproductivity and deep water circulation in the eastern South Atlantic Ocean: evidence from benthic foraminifera. Palaeogeogr. Palaeoclimatol. Palaeoecol. 130, 43–80.

Schmiedl, G., Mackensen, A., Müller, P.J., 1997. Recent benthic foraminifera from the eastern South Atlantic Ocean: dependence on food supply and water masses. Mar. Micropaleontol. 32, 249–287.

Schnitker, D., 1994. Deep Sea benthic foraminifers: food and bottom water masses. In: Zahn, R. (Ed.), Carbon Cycling in the Glacial Ocean: Constraints on the Ocean's Role in Global Change. Springer-Verlag, Berlin, pp. 539–553.

Schrader, H.-J., Gersonde, R., 1978. Diatoms and silicoflagellates. Micropaleontological Counting Methods and Techniques: an Exercise on an Eight Metres Section of the Lower Pliocene of Capo Rosello, Sicily 17.

Schröder, C., Scott, D.B., Medioli, F.S., 1987. Can smaller benthic foraminifera be ignored in paleoenvironmental analyses? J. Foraminifer. Res. 17, 101–109.

Schwager, C., 1866. Fossile Foraminiferen von Kar Nikobar, Reise der Oesterreichischen Fregatte Novara um Erde in den Jahren 1857, 1858, 1859 unten den Befehlen des Commodore B. Von Wuellerstorf-Urbair. Geologischer Theil, Geologische Beobachtung no. 2, Palaeontologische Mittheilung 2, pp. 187–268.

Sen Gupta, B.K., Machain-Castillo, M.L., 1993. Benthic foraminifera in oxygen-poor habitats. Mar. Micropaleontol. 20, 183–201.

Street-Perrott, F.A., Perrott, R.A., 1990. Abrupt climate fluctuations in the tropics: the influence of Atlantic Ocean circulation. Nature 343, 607–612.

Stuut, J.-B.W., Zabel, M., Ratmeyer, V., Helmke, P., Schefuß, E., Lavik, G., Schneider, R.R., 2005. Provenance of present-day eolian dust collected off NW Africa. J. Geophys. Res. 110 http://dx.doi.org/10.1029/2004JD005161.

Suhr, S.B., Pond, D.W., 2006. Antarctic benthic foraminifera facilitate rapid cycling of phytoplankton-derived organic carbon. Deep-Sea Res. II 53, 895–902.

Svensson, A., Andersen, K.K., Bigler, M., Clausen, H.B., Dahl-Jensen, D., Davies, S.M., Johnsen, S.J., Muscheler, R., Parrenin, F., Rasmussen, S.O., Röthlisberger, R., Seierstad, L., Steffensen, J.P., Vinther, B.M., 2008. A 60,000 year Greenland stratigraphic ice core chronology. Clim. Past 4, 47–57.

Sweetman, A.K., Sommer, S., Pfannkuche, O., Witte, U., 2009. Retarded response by macrofauna-size foraminifera to phytodetritus in a deep Norwegian fjord. J. Foraminifer. Res. 39, 15–22.

Tjallingii, R., Claussen, M., Stuut, J.-B.W., Fohlmeister, J., Jahn, A., Bickert, T., Lamy, F., Rohl, U., 2008. Coherent high- and low-latitude control of the northwest African hydrological balance. Nat. Geosci. 1, 670–675.

Tyson, R.V., Pearson, T.H., 1991. Modern and ancient continental shelf anoxia: an overview. In: Tyson, R.V., Pearson, T.H. (Eds.), Modern and Ancient Continental Shelf Anoxia, Geology Society London Special Publications, pp. 1–24.

Vörösmarty, C.J., Fekete, B.M., Meybeck, M., Lammers, R.B., 2000. Global system of rivers: its role in organizing continental land mass and defining land-to-ocean linkages. Glob. Biogeochem. Cycles 14, 599–621.

Weldeab, S., Lea, D.W., Schneider, R.R., Andersen, N., 2007. 155,000 years of West African monsoon and ocean thermal evolution. Science 316, 1303–1307.

Weltje, G., 1997. End-member modelling of compositional data: numerical-statistical algorithms for solving the explicit mixing problem. J. Math. Geol. 29, 503–549.

Weltje, G.J., Prins, M.A., 2003. Muddled or mixed? Inferring palaeoclimate from size distributions of deep-sea clastics. Sediment. Geol. 162, 39–62.

Weltje, G.J., Tjallingi, R., 2008. Calibration of XRF core scanners for quantitative geochemical logging of sediment cores: Theory and application. Earth and Planet. Sci. Lett. 274, 423–438.

Wilson, I.G., 1971. Desert sandflow basins and a model for the development of ergs. Geogr. J. 137, 180–198.

Zarriess, M., Mackensen, A., 2010. The tropical rainbelt and productivity changes off northwest Africa: a 31,000-year high-resolution record. Mar. Micropaleontol. 76, 76–91.

Zhao, M., Eglinton, G., Haslett, S.K., Jordan, R.W., Sarnthein, M., Zhang, Z., 2000. Marine and terrestrial biomarker records for the last 35,000 years at ODP site 658C off NW Africa. Org. Geochem. 31, 919–930.